iScience

CellPress
OPEN ACCESS

Article

Bismuth Porphyrin Antagonizes Cisplatin-Induced Nephrotoxicity *via* Unexpected Metallothionein-Independent Mechanisms

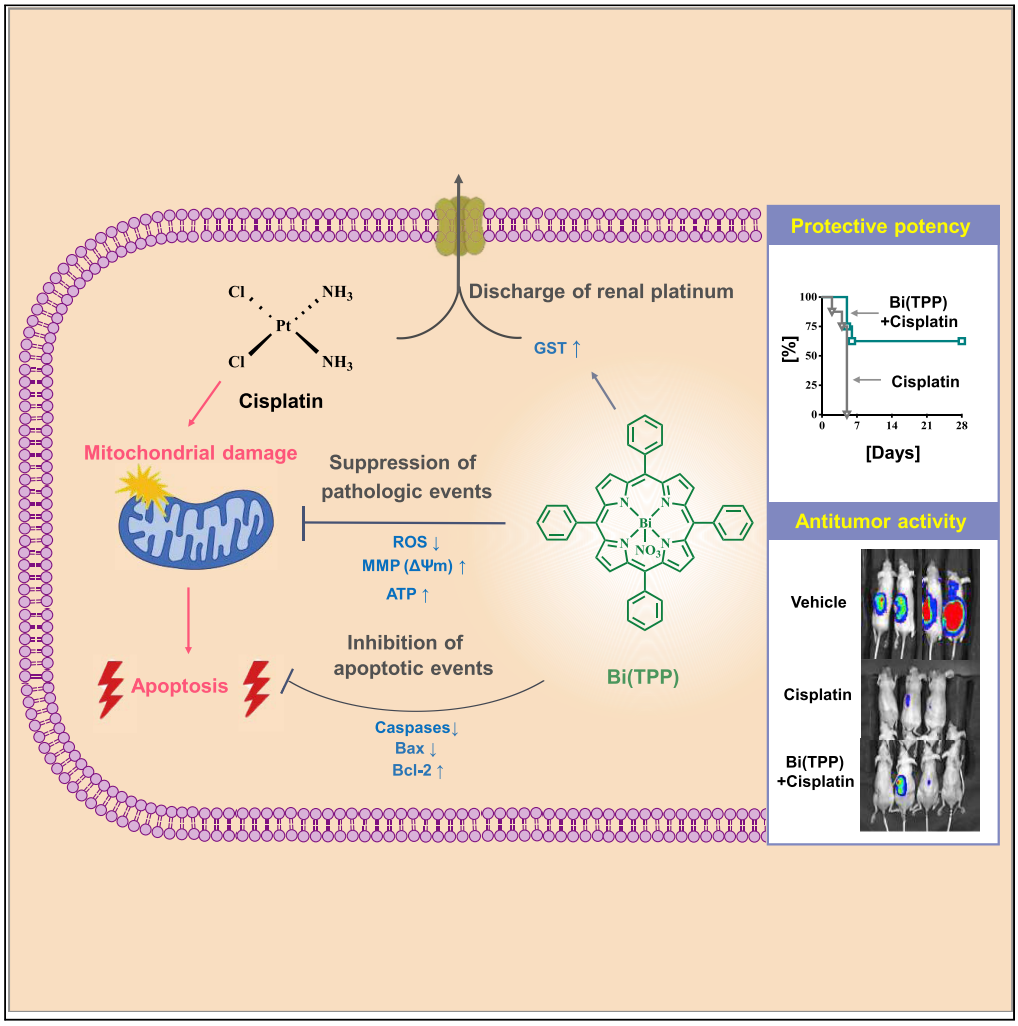

Runming Wang, Suyu Wang, Shing Chan, ..., Godfrey Chi-Fung Chan, Hongyan Li, Hongzhe Sun

hsun@hku.hk

HIGHLIGHTS

Bi(TPP), a potent nephroprotectant against cisplatin-induced toxicity, is disclosed

Protective potency of Bi(TPP) could be modulated by varying lipophilic TPP ligands

Bi(TPP) ameliorates cisplatin-induced renal damage via multiple mechanisms

Combined therapy with Bi(TPP) does not compromise the antitumor efficacy of cisplatin

Wang et al., iScience *23*, 101054
May 22, 2020
https://doi.org/10.1016/j.isci.2020.101054

iScience

CellPress
OPEN ACCESS

Article

Bismuth Porphyrin Antagonizes Cisplatin-Induced Nephrotoxicity *via* Unexpected Metallothionein-Independent Mechanisms

Runming Wang,[1] Suyu Wang,[1] Shing Chan,[2] Yuchuan Wang,[1] Yufeng Zhang,[3] Zhong Zuo,[3] Godfrey Chi-Fung Chan,[2] Hongyan Li,[1] and Hongzhe Sun[1,4,*]

SUMMARY

Cisplatin (CDDP) has been a highly successful anticancer drug in cancer therapy; however, its further application suffers severe nephrotoxicity. Herein, we identify bismuth tetraphenylporphyrinate [Bi(TPP)] as a potent protective agent against CDDP-induced nephrotoxicity. Bi(TPP) attenuates CDDP-induced acute kidney injury and prevents the death of mice exposed to a lethal dose of CDDP. The protective potency of bismuth porphyrin complexes could be optimized by varying lipophilic TPP ligands with ideal ClogP values of 8–14. Unexpectedly, Bi(TPP) exhibited a protective role *via* metallothionein-independent pathways, i.e., maintenance of redox homeostasis and energy supplement, elimination of accumulated platinum in the kidney, and inactivation of caspases cascade in apoptotic pathway. Significantly, Bi(TPP) does not compromise the antitumor activity of CDDP in the orthotopic tumor xenograft mouse model. These findings suggest that Bi(TPP) could be incorporated into current CDDP-based cancer therapy as a nephroprotective agent.

INTRODUCTION

Cisplatin, cis-diamminedichloroplatinum(II) (CDDP), plays a pivotal role in cancer therapy and has been a standard component in the treatment regimens of a wide spectrum of solid tumors including bladder, cervix, head and neck, esophageal, small cell lung cancer, breast cancers, testicular cancer, and neuroblastoma (Bertolini et al., 2009; Cheng et al., 2018; Ladenstein et al., 2020; Seiwert et al., 2007; Silver et al., 2010). It has also been used as salvage therapy in the case that the first-line treatment has failed or in specific situations that preclude the standard treatment (Candelaria et al., 2006; Hausheer et al., 2010). Despite its therapeutic success, CDDP unfortunately exhibits undesirable dose-dependent side effects such as neurotoxicity, ototoxicity, nausea/vomiting, hepatotoxicity, and particularly nephrotoxicity (Rabik and Dolan, 2007). Patients may suffer a progressive and persistent decline in renal function after a successive treatment cycle, which is characterized by a deterioration in the glomerular filtration rate (GFR), massive renal electrolytes loss, and elevated serum urea and creatinine levels (Pabla and Dong, 2008). CDDP-induced nephrotoxicity accounts for up to 60% of all cases of hospital-acquired acute kidney injury (AKI), a disease that is associated with considerable morbidity and mortality (Murugan and Kellum, 2011) and has no effective treatment currently.

Although the precise mechanisms involved in CDDP-induced renal failure have not been thoroughly understood, it is generally believed to be multifaceted including injury to nuclear and mitochondrial DNA, production of reactive oxygen species (ROS)/reactive nitrogen species (RNS), activation of apoptosis, initiation of inflammatory response, and altered transport of CDDP into renal epithelial cells (Wang and Lippard, 2005). Moreover, it was found that platinum is preferentially accumulated in the S3 segment of tubular epithelial cells in kidney being 5-fold concentrated than that in blood (Chevalier, 2016), and a lack of means to eliminate excessive Pt(II) in kidney sharply compromises its therapeutic advantage. Despite various methods used to reduce the side effects caused by CDDP, e.g. pre-hydration with mannitol or furosemide, and co-administration with cimetidine or amifostine (Sprowl et al., 2013), their protective profile are suboptimal and a gap in reducing CDDP-induced nephrotoxicity still remains in the clinic.

Bismuth(III) [Bi(III)] compounds, e.g. bismuth (sub)nitrate, were found to be effective inducers of metallothionein (MT) and have been demonstrated to offer protection against the nephrotoxicity caused by

[1]Department of Chemistry, The University of Hong Kong, Pokfulam Road, Pok Fu Lam, Hong Kong S.A.R., P.R. China

[2]Department of Paediatrics & Adolescent Medicine, LKS Faculty of Medicine, The University of Hong Kong, Pokfulam Road, Pok Fu Lam, Hong Kong S.A.R., P.R. China

[3]School of Pharmacy, Faculty of Medicine, The Chinese University of Hong Kong, Shatin, New Territories, Hong Kong S.A.R., P.R. China

[4]Lead Contact

*Correspondence: hsun@hku.hk

https://doi.org/10.1016/j.isci.2020.101054

CDDP and doxorubicin (Adriamycin) (Fujiwara and Satoh, 2013; Kaegi and Schaeffer, 1988; Klaassen et al., 2009; Maret, 2008; Satoh et al., 1988; Thirumoorthy et al., 2011). Bismuth is a "green" metal and has been used in clinic for the treatment of various diseases for decades, particularly for *Helicobacter pylori* infection (Li and Sun, 2012). Bismuth also achieves the highest visceral concentrations in proximal tubule epithelial cells of kidney as platinum does (Dresow et al., 1991) but exhibits negligible toxicity in humans, attributable to its glutathione, and multidrug-resistant protein-mediated disposal in mammalian cells (Hong et al., 2015). Thus, there is a great potential for bismuth to be incorporated in cancer chemotherapy to circumvent CDDP-induced nephrotoxicity. It is generally believed that Bi(III) may induce certain cytoprotective biomolecules, i.e., reduced glutathione (GSH) and, in particular MT, which are utilized for the defense of oxidative/nitrosative stress or direct chelation of platinum by MT to ameliorate CDDP-induced nephrotoxicity. However, the precise protective mechanism remains elusive. Moreover, the existing bismuth compounds exhibit relatively low protective efficacy, and new potent neuroprotective agents await to be developed.

Here, we report bismuth tetraphenylporphyrinate [Bi(TPP)] as a potent nephroprotective agent both *in vitro* and *in vivo*. Different from previously reported bismuth compounds, Bi(TPP) exhibits protective roles *via* maintaining ROS and ATP levels and eliminating renal platinum and targeting caspase-dependent apoptosis rather than induction of MT. Notably, Bi(TPP) does not interfere with the antitumor activity of CDDP. Therefore, Bi(TPP) has the potential to be incorporated in cancer therapy as an antidote against CDDP-induced nephrotoxicity.

RESULTS

Identification of Cytoprotective Bi(III) Compounds *In Vitro*

We first prepared Bi(III) compounds by coordinating Bi(III) (as $Bi(NO)_3$) with a series of organic ligands including porphyrin, crown ether, salicylic acid analogs, thiols, etc. (Figure S1). The identity and purity of Bi(III) compounds were confirmed by fast atom bombardment (FAB)/electrospray ionisation (ESI) mass spectrometry and nuclear magnetic resonance spectroscopy (NMR) (see in Supplemental Information). The cytotoxicity of synthesized compounds to two mammalian cells was relatively low, with a half cytotoxic concentration (TC_{50}) over 100 μM (Figure S2). To identify cytoprotective Bi(III) compounds, a primary phenotypic screening was conducted on a normal human renal proximal tubule cells (HK-2). HK-2 cells were pre-incubated with or without Bi(III) compounds at fixed concentration (100 μM) and then exposed to cytotoxic concentrations of CDDP (10 μM) over a period of 48 h. Any compound that showed protective index (PI) > 1, where PI was defined as the ratio of survival rate of cells treated with Bi(III) and CDDP to that of CDDP treated alone and had less than 10% cytotoxicity to cells in the absence of CDDP, was considered to be protective. Amifostine, a nephroprotective adjuvant used in cancer chemotherapy, and two reported active compounds, $Bi(NO)_3$ (Boogaard et al., 1991) and BiZn (Chan et al., 2019), as well as three bismuth drugs, i.e., bismuth subsalicylate (BSS, Pepto-Bismol), colloidal bismuth subcitrate (CBS, De-Nol), and bismuth subgallate (BSG, Devrom) were used for comparison. This primary screening generated two categories of active compounds, i.e., Bi(III) tetraphenylporphyrate (Cpd 1) and Bi(III) thiolates (Cpd 6 and Cpd 8) with PI of 3.54, 2.82, and 2.90 for HK-2 cells, respectively. These compounds had much higher PI than amifostine and other Bi(III) compounds with PI no greater than 2 (Figure 1A). We further demonstrated that Cpd 1 [Bi(TPP)] and Cpd 8 [$Bi(NAC)_3$] (Figure 1B) protected cells in a dose-dependent manner with the protective potency (EC_{50}) of 15.3 and 73.7 μM for HK-2 cells, respectively, under identical conditions (Figures 1C and 1D).

In Vivo Protective Potency of Bi(III) Compounds in Mouse Model of CDDP-Induced Kidney Injury

We further evaluated the protective effect of selected Bi(III) compounds on CDDP-induced renal toxicity in a validated mouse model of acute kidney injury. Briefly, groups of mice receiving intraperitoneal injection of a lethal dose (20 mg kg^{-1}) of CDDP were administered orally with Bi(III) compounds three times prior to and twice after CDDP treatment as shown in Figure 2A. The administration of CDDP led to acute renal damage with 10-fold increase in the level of renal toxicity biomarker, blood urea nitrogen (BUN), from 17.7 to 171.1 mg dL^{-1} in comparison to non-treated group (Figure 2B). The BUN levels were reduced greatly by co-administration with all the three tested compounds, among which Bi(TPP) showed the highest nephroprotective potency with the upregulated BUN level being recovered by ~2.83 folds. No or negligible increase in BUN level was noted when they were used alone, indicative of the non-nephrotoxicity of the tested compound (Figure 2B). The renal platinum levels were determined 3 days after CDDP injection, and approximately 47.2% decrease in the platinum level was noted in the mouse kidney of Bi(TPP) co-treatment group

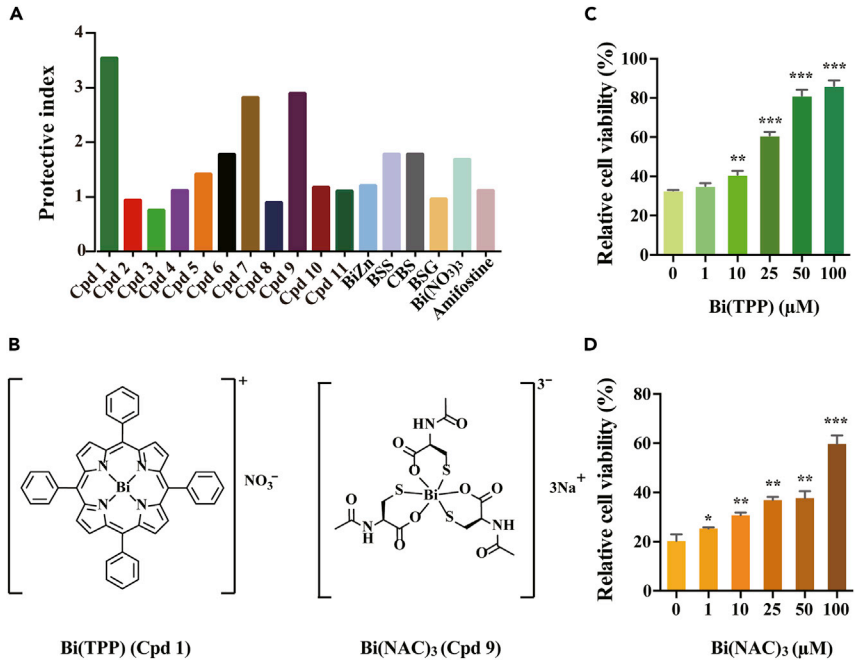

Figure 1. *In Vitro* Screening Identifies Bismuth Compounds with Nephroprotective Effects on Kidney Cells

(A) Bar chart illustrating the representative protective index of Bi(III) compounds for HK-2 cells.

(B) The proposed structures of selected bismuth compounds, Bi(TPP) and $Bi(NAC)_3$.

(C and D) The dose-dependent protective effects of (C) Bi(TPP) and (D) $Bi(NAC)_3$ for HK-2 cells. Data are represented as mean ± SEM. *$p < 0.05$ **$p < 0.01$, and ***$p < 0.001$, Student's t test, with the significance in comparison to the group of Bi(III) concentration at 0 μM.

compared with those of CDDP-alone group (Figure 2C), indicating that Bi(TPP) could facilitate platinum clearance from renal cells. In a separate experiment, acute renal damage induced by CDDP resulted in around 30% body weight loss 4 days after CDDP treatment (Figure 2D) and further led to death of all mice within five days (Figure 2E). In contrast, pre-treatment of Bi(TPP) effectively prevented the death of mice with a survival rate of 66.7%, whereas $Bi(NAC)_3$ and BiZn could only rescue 12.5% and 25% of mice, respectively, at the end of the experimental period (Figure 2E). The body weights of survived mice were recovered to normal ranges within four weeks (Figure 2D).

Oral administration of Bi(TPP) as a representative compound was studied in mice to preliminarily evaluate the pharmacokinetics profile of related Bi(III) compounds. The compound was administered to mice orally. The plasma and kidney of the mice were sampled between 0 and 48 h at different time intervals shown in Figure 2F. Bi(TPP) displayed a rapid absorption profile with maximum concentration of 16.8 $\mu g\ L^{-1}$ (C_{max}) reached at 1 h (T_{max}). $AUC_{0-48\ h}$ of Bi(TPP) could achieve 370.2 $h \cdot \mu g\ L^{-1}$ with an estimated plasma $t_{1/2}$ of 6 h (Table S1). The renal bismuth content was also profiled over the period of 48 h as shown in Figure 2G, demonstating the sufficient accumulation of bismuth in kidney.. Taken together, we showed that the tested Bi(III) compounds, in particular Bi(TPP), served as a protective agent against CDDP-induced renal toxicity in mice.

Structure and Activity Relationship of Bi(III) Porphyrins

To explore the role of Bi(III) and porphyrin ligand, we first compared the protective effect of Bi(TPP) with other metallo-tetraphenylporphyrinates in HK-2 cells. As shown in Figure 3A, porphyrinates of Fe(III), Cu(II), Co(II), and Zn(II) were also identified to be active with protective index of around 3, whereas negligible or no protection was provided by porphyrinates of either Mn(III) or Ga(III) or the ligand itself. Nevertheless, the protective index of Bi(TPP) was determined to be the best with the highest PI value. We then examined structure-activity relationship (SAR) of Bi(III) porphyrinates and synthesized a series of Bi(III) compounds by complexation with tetraphenylporphyrin and its derivatives (Figure 3B) as described in the Material and Method section. The *in vitro* screening gave rise to seven Bi(III) porphyrinates with PI values

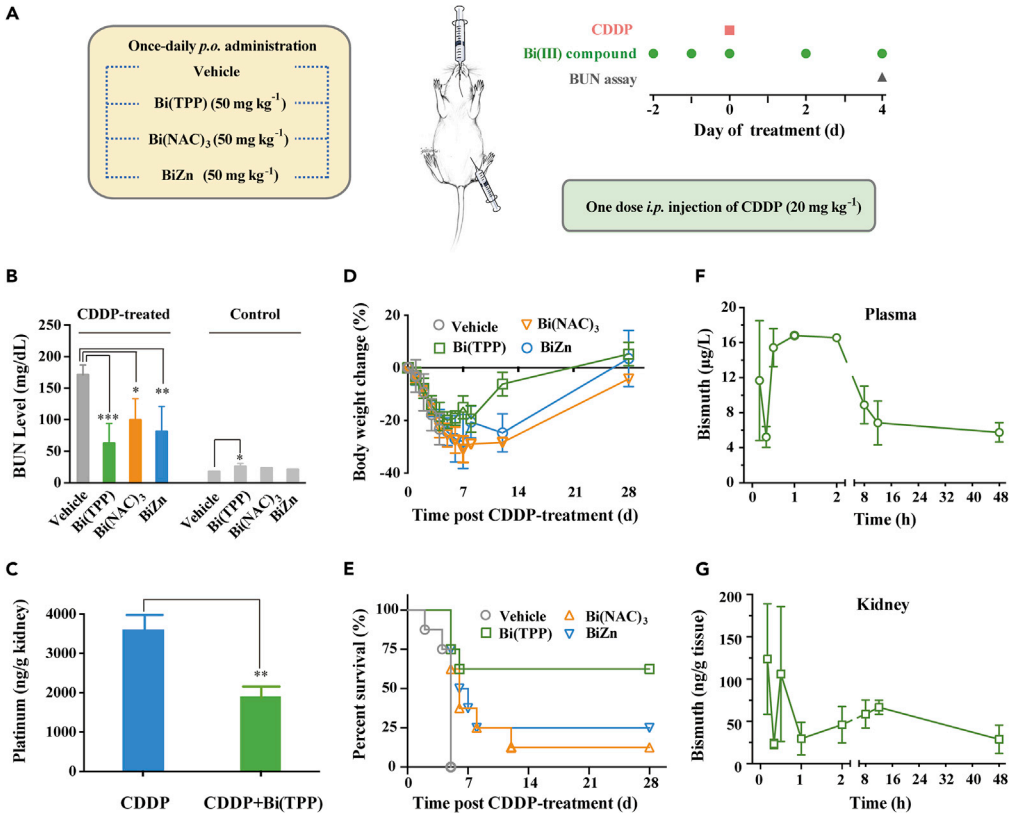

Figure 2. Bismuth Compounds Exerts *In Vivo* Protective Potency against CDDP-induced Renal Damage

(A) Schematic representation of the experimental design. Groups of mice were orally administered with Bi(TPP), $Bi(NAC)_3$, and BiZn, respectively and then intraperitoneally administered with CDDP. Mice treated with vehicle, Bi(TPP), $Bi(NAC)_3$, or BiZn in the absence of CDDP served as control.(B) Bar chart showing the BUN level of groups of mice treated versus untreated with Bi(TPP), $Bi(NAC)_3$, and BiZn upon the treatment of CDDP. Data are represented as mean ± SEM. *$p < 0.05$ **$p < 0.01$, and ***$p < 0.001$, Student's t test.(C) Renal platinum levels were measured in the kidneys of mice from CDDP-alone and CDDP-Bi(TPP) co-administration group three days after CDDP injection. Data are represented as mean ± SEM; n = 4 for CDDP group and n = 6 for CDDP-Bi(TPP) co-administration group; **$p < 0.01$, Student's t test.(D) Curves of averaged body weight changes of each group after CDDP injection. Error bars represent means ± SEM from biological replicates.(E) Survival curves showing the protective effects of Bi(TPP) and $Bi(NAC)_3$. Eight mice per treatment group were used for the survival studies. $p < 0.001$, Mantel-Cox test.(F and G) Pharmacokinetics profiles of (F) plasma bismuth concentration and (G) renal bismuth content. Bi(TPP) was used at 50 mg kg^{-1} following oral administration. Three mice were used for each time point, and data are represented as mean ± SEM.

of 1.84–4.58 and three compounds with PI lower than 1 (Figure 3C). The protective activity and the ClogP of the ligands could be approximately fitted into a third-order equation as shown in inset of Figure 3C, suggesting that the protective activity of Bi(III) porphyrinates could be finely tuned by altering the lipophilicity of the ligand. Generally, a lipophilic porphyrin ligand with Clog P ranged from 8 to 14 may favor the activity of the compound, as the increased lipophilicity facilitated the passive permeation of small molecules (Arnott and Planey, 2012). The protective effectiveness of two of the most potent Bi(III) complexes with TPP derivatives, Bi(TMOPP) and Bi(TMPP), were further verified in the mouse model under identical condition, as shown in Figures 3D and 3E. Collectively, we showed that the protective effectiveness of Bi(III) porphyrinate could be optimized by tuning ligand lipophilicity.

Buffering of CDDP-Regulated Gene Alteration in Key Biological Pathways by Bi(TPP)

To gain a global perspective of the protective mechanism(s) of Bi(TPP) toward CDDP-induced nephrotoxicity, we performed transcriptomic analysis on the kidneys of mice treated with either Bi(TPP) (and BiZn for comparison), CDDP, or their combinations. In comparison to vehicle-treated group, CDDP severely altered the transcriptome level of mouse kidney with 2,453 genes being upregulated and 2,250 genes being

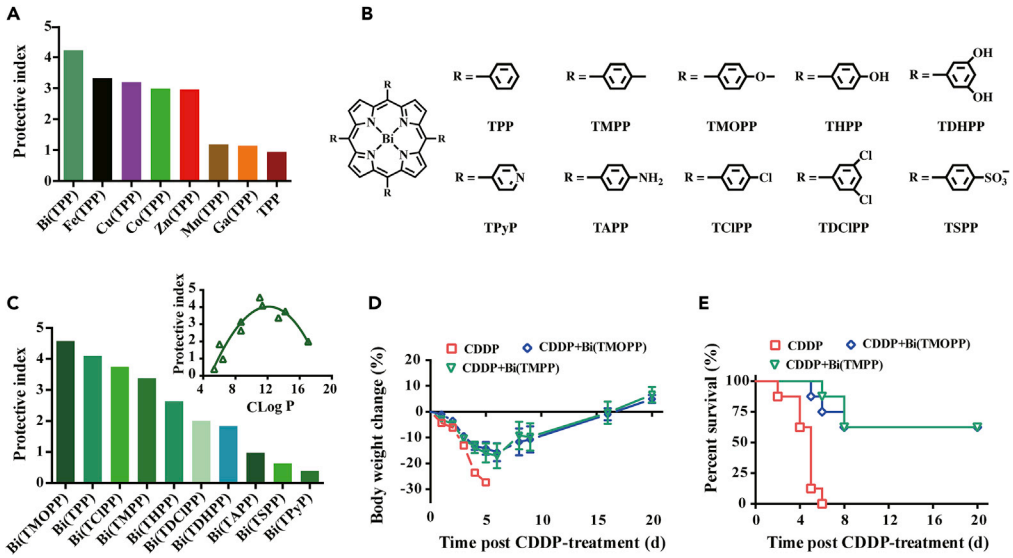

Figure 3. Protective Potency of Bismuth Porphyrin Complexes Could Be Optimized by Varying Lipophilic TPP Ligands

(A) Comparison of protective effects of Bi(III)- and other metallo-porphyrins. Bi(TPP) derivatives were synthesized with ligands shown in (B) and their protective activity is shown in (C), with the correlation between protective index of the Bi(III) compounds and ClogP of related porphyrin ligands shown as the inset. (D and E) *In vivo* protective performance of Bi(TMOPP) and Bi(TMPP) is shown as averaged body weight change (D) Error bars represent means ± SEM from biological replicates. and survival rate (E). Eight mice per treatment group were used for the survival studies. $p < 0.001$, Mantel-Cox test.

downregulated ($p < 0.05$). However, the co-administration of Bi(TPP) significantly suppressed the upregulated genes by 29.2% (717) and the downregulated genes by 28.7% (646) as shown in the heat maps in Figure 4A, SET I, and Figure 4B, SET II, respectively. In contrast, BiZn could only buffer 11.2% (275) and 9.1% (204) genes that were up- and downregulated by CDDP, respectively (Figures S3A and S3B), in line with its inferior *in vivo* effectiveness to Bi(TPP) as demonstrated earlier. We then examined the expression levels of GSH- and MT-related genes, which were previously considered to be responsible for the protective role of Bi(III) for CDDP-induced nephrotoxicity. We found that GSH-related genes including *Mgst1* and *Mgst2* and MT-related genes including *Mt1* and *Mt2* were significantly upregulated in BiZn-treated group (Figure 4C). The expressions of some genes were further induced when BiZn and CDDP were used together, including *Gsta3* (1.19 folds), *Gsta4* (1.76 folds), *Gstm6* (3.22 folds), *Mgst1* (2.76 folds), *Mgst2* (8.90 folds), *Mt1* (19.73 folds), and particularly *Mt2* (42.06 fold) (Figures 4C and Table S2). These results are in agreement with previous reports that the significant upregulation of GSH and MT in kidney contributed greatly to the nephroprotection provided by BiZn and related Bi(III) compounds, e.g. BN, BSN, and CBS (Boogaard et al., 1991; Kondo et al., 2004; Leussink et al., 2003; Naganuma et al., 1987). In contrast to BiZn, Bi(TPP) suppressed the expression of *Mgst2* by 2.34-fold and slightly induced the expression of *Gstt1*, *Gstt2*, *Gstm6*, *Gstm7*, and *Gsta2* by no more than 1.6-fold (Figure 4C and Table S2). We then compared the expression levels of these genes in the CDDP-alone group with those of the CDDP-Bi(TPP) combination group and found that the genes related to GSH and MT were not significantly upregulated. Instead, the expression of *Mt1* and *Mt2* were largely suppressed to almost normal levels (Table S2). These results suggest the protection provided by Bi(TPP) may represent a new mechanism.

Gene ontology (GO) network was created to probe the functional specificity of clusters differentiated between CDDP-alone and CDDP-Bi(TPP) combination groups with respect to biological processes. Genes in SET I were functionally arranged into 15 parental clusters, and the most significantly enriched two clusters were genes related to endopeptidase activity (GO:0004175) and regulation of protein phosphorylation (GO:0001932) with 26 and 24 child terms, respectively (Figures 4D and S3C and Table S3). Although the genes in SET II were grouped into 15 clusters among which inorganic cation transmembrane transporter activity (GO:0022890) with 12 child terms was the most significantly enriched cluster (Figures 4F and S3D and Table S4). The child-annotated terms in endopeptidase activity could be predominantly traced to

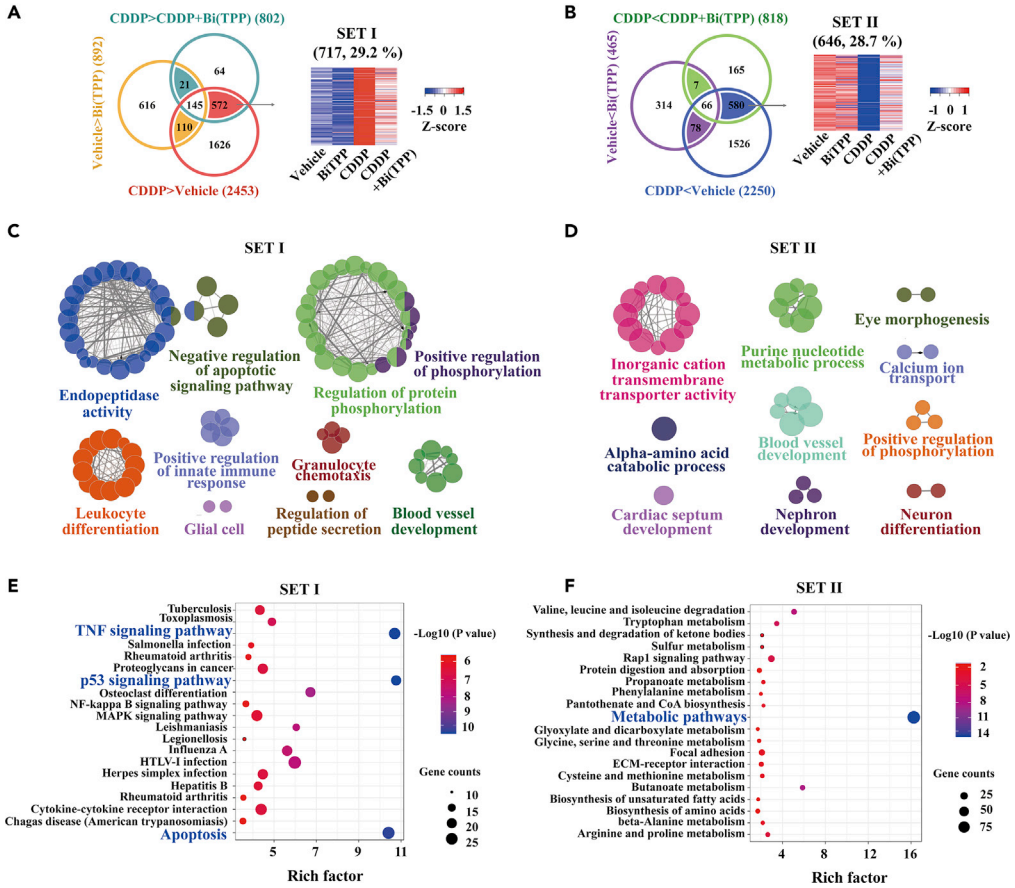

Figure 4. Whole Transcriptome Analysis Reveals the Nephroprotective Mode of Action of Bi(TPP)

(A and B) Venn image and heatmap of whole transcriptome sequencing on kidney extracts from mice receiving treatments of vehicle, Bi(TPP), CDDP, or CDDP + Bi(TPP), n = 3 animals per group. The overlapping sets amid Venn image revealing that the expression of genes (A) in SET I was suppressed over CDDP-induced upregulation and (B) in SET II was induced over CDDP-induced downregulation upon the treatment of Bi(TPP). Heat maps illustrate the scaled average gene expression. A false discovery cut-off rate = 0.05 was used for determining differential gene expression. Blue color indicates low expression, whereas red color indicates high expression.

(C and D) Cytoscape analysis showing overrepresented biological process from GO analysis for genes in (C) SET I and (D) SET II. Colors represent the GO group. GO analysis and visualization was performed using the ClueGo Cytoscape plug-in. GO terms are presented as nodes and are clustered together based on the similarity of genes present in each term or pathway. Nodes with multiple colors are associated with more than one process.

(E and F) Bubble charts showing KEGG pathway that are significant for genes in (E) SET I and (F) SET II ($p < 0.05$). KEGG pathway enrichments are displayed in a scatter diagram, where each point represents the enrichment level, color corresponds to the q-value, and the size corresponds to the number of genes enriched for the given pathway. Red indicates the q-value; the smaller the value, the more significant the pathway enrichment.

cysteine-type endopeptidase activity involved in apoptotic process (GO:0097153), which were in close relation to another parent cluster, negative regulation of apoptotic signaling pathway (GO:2001234) as showed in Figure S3C. This provided clues that Bi(TPP) may generically regulate the activity of cysteine-type endopeptidase related to apoptosis process. The genes upregulated by Bi(TPP) were largely related to the annotated term of cation transmembrane transporter activity, wherein gene expression levels of multidrug and toxin extrusion 1 transporter *MATE1/SLC47A1* and copper efflux transporters *ATP7A* and *ATP7B* were increased by 1.23-, 1.41-, and 1.33-folds, respectively (Table S2). The former has been demonstrated to efflux CDDP into the tubular lumen, thus reducing cellular accumulation of CDDP (Nakamura et al., 2010) and the latter to sequester CDDP into subcellular compartments, limiting CDDP cytotoxicity (Leonhardt et al., 2009; Samimi et al., 2004). Additionally, the significantly enriched GO terms in SET II genes include acyl-CoA metabolic process (GO:0006637), purine ribonucleotide metabolic process (GO:0009150), fatty acid biosynthetic process (GO:0009062), kidney epithelium development (GO:0072073), and nephron

epithelium development (GO:0072006) (Figure S3D), indicating that the action of Bi(TPP) may be associated with cell proliferation and cell respiration.

A Kyoto Encyclopedia of Genes and Genomes (KEGG) enrichment analysis showed that genes in SET I are primarily enriched in p53 signaling pathway (20 gene counts, $p = 1.70 \times 10^{-11}$), TNF signaling pathway (24 gene counts, $p = 1.99 \times 10^{-11}$), and apoptosis pathway (26 gene counts, $p = 3.90 \times 10^{-11}$) among the 245 annotated KEGG pathways (Figure 4F and Table S5), whereas genes in SET II are primarily enriched in metabolic pathways (96 gene counts, $p = 2.87 \times 10^{-17}$) among 235 KEGG pathways (Figure 4G and Table S6). The differentially expressed genes from the four most enriched pathways were further shown as $\log_2$FPKM value of CDDP-Bi(TPP) combination versus CDDP-alone group (Figure S3E). We found that genes encoding TNF-alpha and several key cysteine-containing pro-apoptotic proteins (Bax, caspase 7, caspase 8) involved in caspase cascade in TNF-induced apoptosis pathway were significantly downregulated. Genes encoding proteins belonging to cytochrome P450 superfamily (*CYP2C44*, *CYP2A5*, *CYP51*, *CYP4F14*), which serves as drug metabolism mediators, were upregulated as shown in Figure S3E and Table S2. This was in accordance with CYP-mediated drug clearance *in vivo* as reported previously (Backman et al., 2016; Quintanilha et al., 2017).

Modulation of CDDP-Induced Oxidative Stress, Energetic Metabolism Impairment by Bi(TPP)

The Bi(TPP)-induced alteration in mRNA expression levels was confirmed in HK-2 cells by reverse-transcriptase PCR (RT-PCR). According to the RT-PCR data shown in Figure 5A, the expression levels of *MT1A*, *MT2A*, and *SLC22A1* were slightly increased by 2.30-, 2.62-, and 1.65-folds, respectively, whereas that of cytochrome P450 superfamily (*CYP2C44*, *CYP2A5*, *CYP51*, *CYP4F14*) were generally upregulated by more than 3-fold. In contrast, the expression level of *SLC47A1* was increased by 19.6-fold, which may refer to enhanced effluxing capacity toward CDDP (Nakamura et al., 2010). Interestingly, we observed that the gene expression levels of glutathione-S-transferases (GSTs) were dramatically increased at cellular level, in particular that of *GSTA1*, *GSTA3*, and *GSTM5* being increased by 39.9-, 454.9- and 28.5-fold, respectively. GSTs are a family of multifunctional enzymes that could modulate CDDP-induced generation of ROS by catalyzing the conjugation of GSH with electrophilic substrates (De Luca et al., 2019; Hayes et al., 2005). Any ROS accumulation beyond the cellular antioxidant capacity depolarizes mitochondrial membrane potential ($\Delta\Psi$m, MMP), a marker for mitochondrial activity, and subsequently leads to a compromised adenosine triphosphate (ATP) production *in cellulo* (Godbout et al., 2002; Kruidering et al., 1997).

GST activity was measured in HK-2 cells by spectrometrically monitoring GST-catalyzed reaction between GSH and the GST substrate, CDNB (1-chloro-2,4-dinitrobenzene), to produce a GS-DNB conjugate. The treatment of Bi(TPP) led to the increase of activity from 46.8 to 95.4 μmol min^{-1} per 10^6 cells in a dose-dependent manner (Figure 5B). This corresponded with the RT-PCR data that Bi(TPP) induced the production of GST. The cellular ROS level was increased to 174.5% after exposure of HK-2 cells to CDDP for 24 h. However, such an increase was almost completely prevented by Bi(TPP) at 10 μM or higher concentrations (Figure 5C). We next examined the cellular MMP and ATP levels. Bi(TPP) ameliorated the loss of mitochondrial membrane potential ($\Delta\Psi$m, MMP) caused by CDDP and scarcely altered $\Delta\Psi$m when used alone (Figure S4). Bi(TPP) increased the ATP level from 148.5 to 222.1 nM/10^4 cells in a dose-dependent manner (Figure 5D). Notably, in a separate experiment, we observed greatly reduced cellular platinum level by nearly 4-fold upon pretreatment of cells with Bi(TPP) at 100 μM (Figure 5E). This was in accordance with the diminished renal platinum level found in mice (Figure 2C), which may be due to the formed GS-platinum complex, bis-(glutathionato)-platinum(II) being effluxed from renal cells in an ATP-dependent manner(Ishikawa and Ali-Osman, 1993; Renes et al., 1999).

Amelioration of CDDP-Induced Caspase-Dependent Apoptosis by Bi(TPP)

Based on bioinformatics analysis, we further explore the Bi(TPP)-mediated detoxification in caspase-dependent apoptosis pathway. It has been demonstrated that CDDP-induced nephrotoxicity occurred primarily through programmed cell death (apoptosis) (Cummings and Schnellmann, 2002; Gonzalez et al., 2001). We then examined the apoptosis of CDDP treated HK-2 cells with or without pretreatment of Bi(TPP) and Zn(TPP) by flow cytometry. We found that CDDP-Bi(TPP) treatment markedly induced cell proliferation by 79.6%, whereas pretreatment of Zn(TPP) led to cell proliferation by 57.4%, similar to that of CDDP treatment alone (53.2%). In accordance, significant reduction in the percentage of cells undergoing apoptosis to 10.5% was observed in Bi(TPP)-CDDP treatment; in comparison, 23.6% and 36.8% of cell apoptosis were noted in Zn(TPP)-CDDP and CDDP-only groups, respectively (Figure 6A), indicating the pretreatment of Bi(TPP) prevents cells from apoptosis.

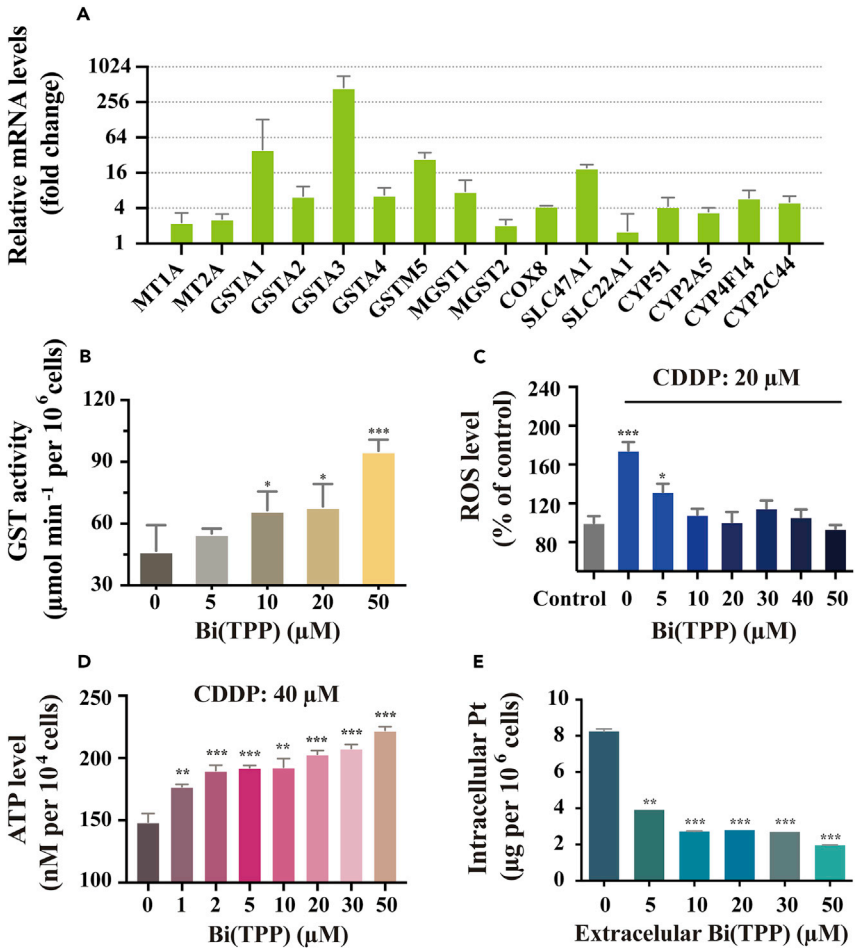

Figure 5. Bi(TPP) Modulates CDDP-Induced Oxidative Stress, Energetic Metabolism Impairment

(A) The relative fold changes of the expression levels for selected genes in HK-2 cells after Bi(TPP) (10 μM) treatment in comparison to non-treated group, which was determined by RT-PCR.

(B) GST activity determination in HK-2 cells after treatment with Bi(TPP) at gradient concentrations.

(C) Cellular ROS levels in HK-2 cells after treatment with CDDP (20 μM) or CDDP in combination with a range of Bi(TPP) concentrations.

(D) ATP levels in HK-2 cells after treatment with CDDP (40 μM) or CDDP in combination with gradient concentrations of Bi(TPP).

(E) Platinum content in HK-2 cells exposed to a range of Bi(TPP) concentrations. (B–E) Mean value of three replicates are shown, and error bars represent means ± SEM in experiment above. *$p < 0.05$, **$p < 0.01$, and ***$p < 0.001$, Student's t test, with the significance in comparison to the group of Bi(TPP) concentration at 0 μM for (B, D, and E) and to control group for (C).

Western blot analysis of HK-2 cells treated with CDDP revealed that TNF, apoptotic regulator Bax, and active caspases, i.e., caspase 3, caspase 7, caspase 8, and caspase 9, that mediate cell death in CDDP-induced nephrotoxicity, were upregulated. However, such upregulations were prevented upon supplementation of Bi(TPP) to the cell prior to CDDP treatment, whereas an increase in the expression levels of anti-apoptotic protein Bcl-2 was observed (Figure 6B). Notably, Bi(TPP) did not affect the expression of p53, indicating that the amelioration of CDDP-induced apoptosis by Bi(TPP) was p53 independent. Moreover, we observed dose-dependent effects on the expression levels of caspase 3, caspase 7, caspase 8, caspase 9, Bax, and Bcl-2 upon treatment of cells by varying concentrations of Bi(TPP) in the absence of CDDP (Figure 6C), revealing that Bi(TPP) itself suppressed the apoptotic signaling in cells to a certain extent. Bi(III) has been shown to be able to inhibit enzyme activity in cells *via* binding to key cysteines in the active sites of enzymes (Cun et al., 2008; Wang et al., 2018). We then examined whether Bi(TPP) could target caspases 3/7 in cells. By using cellular thermal shift assay (Jafari et al., 2014), we show that melting temperatures of both

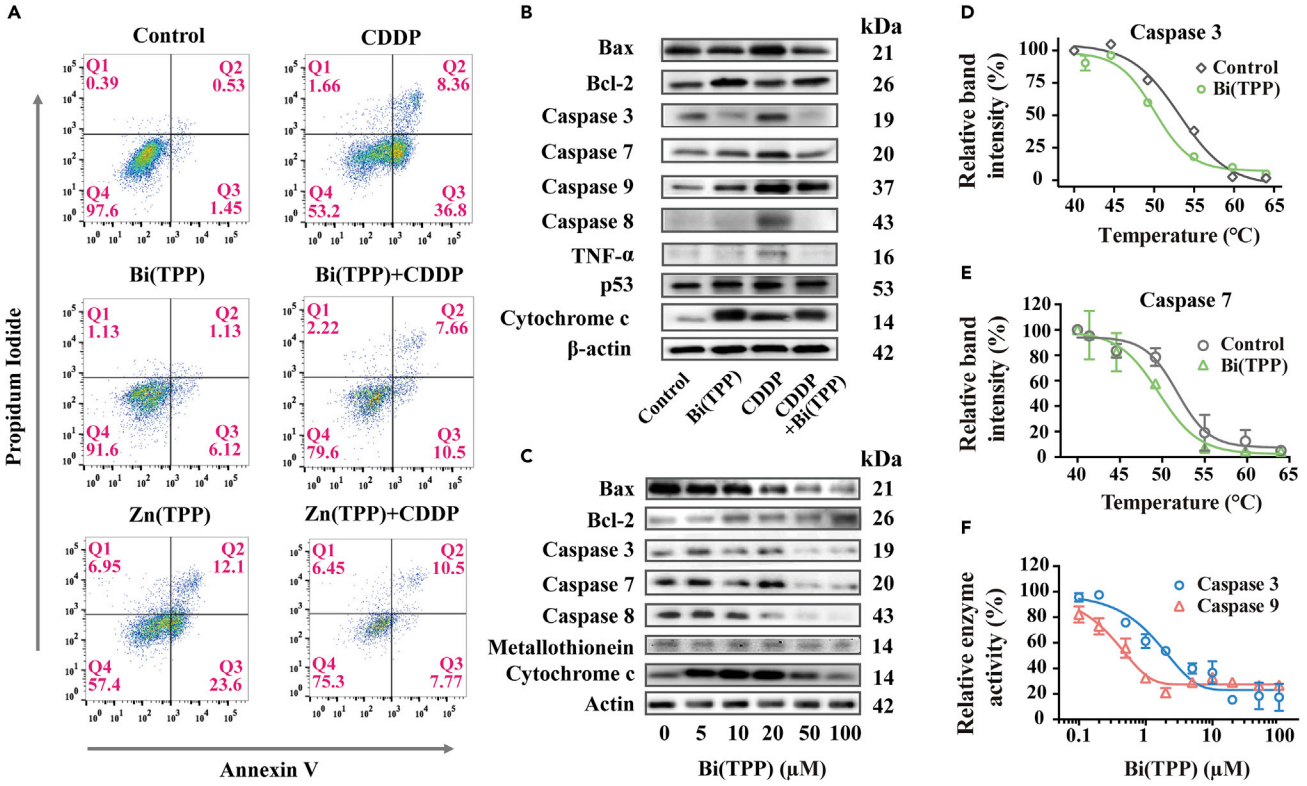

Figure 6. Bi(TPP) Ameliorates CDDP-induced Caspase-dependent Apoptosis

(A) Apoptosis analysis of HK-2 cells upon treatment with vehicle, CDDP, Bi(TPP), Bi(TPP)+CDDP, Zn(TPP), and Zn(TPP)+CDDP by flow cytometry.

(B) Representative immunoblots of HK-2 cells treated with vehicle (DMSO), Bi(TPP) (40 μM), CDDP (20 μM), or their combination for 24 h. Blots were probed with antibodies for Bax (21 kDa), Bcl-2 (26 kDa), caspase 3 (active fragment, 19 kDa), caspase 7 (active fragment, 20 kDa), caspase 8 (active fragment, 43 kDa), caspase 9 (active fragment, 37 kDa), TNF-alpha (16 kDa), p53 (53 kDa), cytochrome *c* (14 kDa), and β-actin (42 kDa).

(C) Dose-dependent manner of blots from HK-2 cells treated with escalating concentrations of Bi(TPP). Antibody of metallothionein1+ metallothionein2 (14 kDa) was used.

(D and E) Cellular thermal shift assays showing the binding of Bi(III) to (D) caspase 3 and (E) caspase 9 in HK-2 cell with ΔTm = 3.10°C and 2.17°C, respectively. Data are represented as mean ± SEM.

(F) Inhibition profiles of caspase 3 and caspase 9 by Bi(TPP) with IC_{50} values of 2.19 μM and 0.53 μM, respectively. Data are represented as mean ± SEM.

caspase 3 and caspase 7 were decreased by Bi(TPP) (Figures 6D and 6E), indicative of binding of Bi(III) to the enzymes. Moreover, we observed the reduced caspase activity in lysate extracted from HK-2 cells treated with Bi(TPP) in the absence of CDDP (Figure S5). We further carried out an enzymatic assay on recombinant proteins and observed that the activity of cleaved caspase 3 and caspase 9 were inhibited by Bi(TPP) with IC_{50} of 2.19 μM and 0.53 μM, respectively (Figure 6F). Our combined data provided evidence that Bi(TPP) protects CDDP-induced cell death by maintaining cellular redox, preserving mitochondrial function, facilitating the excretion of renal platinum, and attenuating caspase-dependent apoptosis.

CDDP Antineoplastic Performance in Neuroblastoma Mouse Pretreated with Bi(III) Compounds

It is of vital importance to examine whether the pre-administration of tested Bi(III) compounds would ameliorate CDDP-induced nephrotoxicity, without interfering with the anti-tumor response of CDDP. We evaluated the antineoplastic activity of CDDP with or without pretreatment of Bi(III) compounds in an orthotopic neuroblastoma xenograft model. The neuroblastoma cells SKNLP were stably transfected with the luciferase gene and orthotopically inoculated at the adrenal area of SCID Beige mice as previously described (Chan et al., 2019). Mice were pre-treated with Bi(III) compounds prior to CDDP treatment as schemed in Figure 7A, and the tumor burden was monitored by bioluminescence imaging. We found that the tumor size was significantly decreased with averaged diameter from 19.3 mm in non-treated group to 6.7 mm in CDDP-alone treatment group for three weeks (Figure 7B).

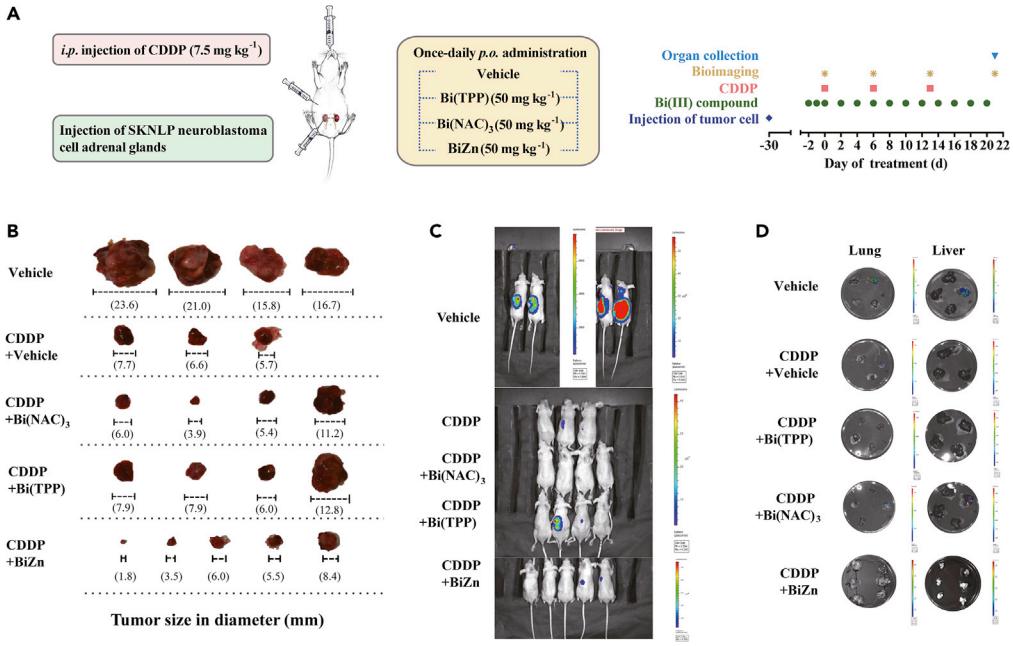

Figure 7. Bi(III) Compounds Does Not Attenuate the Anticancer Properties of CDDP on Adrenal Tumors

(A) Schematic representation of the experimental design.

(B) Photos showing the size of tumor dissected three weeks after CDDP treatment. Four mice were used in vehicle, CDDP + vehicle, CDDP + $Bi(NAC)_3$, and CDDP + Bi(TPP) group; one mouse in CDDP-alone group died owing to the toxicity of CDDP during the experimental period; five mice were used in CDDP + BiZn.

(C) Luminescence images of the SKNLP neuroblastoma cells growth in the identical mice as shown in (B). The scale of luminescent flux is shown in the bar chart right to the luminescence image.

(D) Luminescent scans of dissected liver and lung from the same mice in (B), showing the metastasis of SKNLP cells from adrenal gland to either liver or lung. The scale of luminescent flux is shown in the bar chart right to the luminescence image.

Pre-administration of either Bi(TPP) or $Bi(NAC)_3$ or BiZn led to almost no changes in tumor size, suggesting that pretreatment of Bi(III) compounds have negligible effects on the anti-tumor action of CDDP (Figure 7B). On the contrary, the bioluminescence imaging showed no significant difference in total flux in mice receiving treatment of CDDP alone or CDDP-Bi(III) combination three weeks after treatment completion, which was far lower than that in non-treated group (Figure 7C). Furthermore, no significant tumor metastasis to liver or lung was observed in either CDDP-alone or combination groups, in contrast to non-treated group (Figure 7D). We demonstrated that the tested Bi(III) compounds, i.e., Bi(TPP) and $Bi(NAC)_3$, do not compromise CDDP antineoplastic activity against neuroblastoma, and concurrently nephroprotection role of Bi(TPP) is not due to its capability of sequestration of CDDP in the blood.

DISCUSSION

The use of highly successful anticancer drug CDDP is limited by its severe side effects, in particular nephrotoxicity (Rabik and Dolan, 2007). This nephrotoxicity is mainly attributable to preferential accumulation of CDDP in renal proximal tubules, primarily in the epithelial tubular cells of the S3 segment, which subsequently favors the renal platinum uptake systems (dos Santos et al., 2012). A number of nephroprotective agents have been tested or even put on clinical trial, such as cimetidine (and Imatinib as OCT-2 substrate), amifostine (Ethyol as antioxidants), trichostatin A (and suberoylanilide hydroxamic acid as p53 inhibitor), quercetin (as TNF-α inhibitor), and so on (Cvitkovic, 1998; Katsuda et al., 2010; Tanihara et al., 2009). However, the protective effects of most agents are partial and few of them were not to interfere with antitumor efficacy of CDDP in the experimental context (Koyner et al., 2008). Moreover, some cytoprotectors exert severe adverse effects (Rades et al., 2004). Currently there is no satisfactory strategy to reduce CDDP-induced nephrotoxicity without compromising the anticancer activity of CDDP.

In this study, we identify two protective Bi(III) compounds, Bi(TPP) and $Bi(NAC)_3$, based on a cell-based screening, nevertheless the *in vitro* activity of the latter was not efficiently translated in animal models. Co-administration of Bi(TPP) diminished the renal damage and increased the survival rate of mice receiving a lethal dose of CDDP, thus a high dose of CDDP could be administrated to patients. Our results suggest that once Bi(TPP) is absorbed into the bloodstream, it is rapidly metabolized and distributed to the kidney, during which the plasma bismuth content remains well under the documented safety level (50 $\mu g\ L^{-1}$)) or alarm level (100 $\mu g\ L^{-1}$) (Benet, 1991). The pharmacokinetics profiles show that in comparison to BiZn, Bi(TPP) possessed lower clearance rate and higher AUC_{0-8h} value (104.2 $\mu g\ L^{-1}$ h of Bi(TPP) versus 78.3 $\mu g\ L^{-1}$ h of BiZn) (Table S1), which is in line with its superior protective effectiveness. In this regard, longer duration and less peak-to-trough variations might optimize the dosing frequency and potentially improve oral efficacy.

Porphyrin ligands are well documented to be able to modify the lipophilicity of metal complex, which mediates the membrane permeability of metal complexes and metal uptake *via* passive diffusion in a membrane-potential dependent manner (Haas and Franz, 2009). This is confirmed by our data that the protective potency of Bi(III) porphyrin complexes is correlated with the ClogP value of porphyrin ligands (Figure 3C). Protective potency of Bi(TPP) may be rooted from the metal coordination environments and synergized function with porphyrin ligands. Nevertheless, we conclude that an appropriate lipophilicity is one of the important factors that contributes to the protective potency of Bi(TPP). The precise mode of action(s) among different Bi(III) porphyrin compounds still needs further investigation.

We then perform a comprehensive mechanistic study of the protective role of Bi(TPP) by transcriptome analysis and bioassays. We show that Bi(TPP) confers protection against CDDP-induced nephrotoxicity not primarily owing to the induction of MT (Figures 5A and 6C) but rather to other multiple protective mechanisms. We first observe that the Bi(TPP) induced upregulation of GSTs (Figures 5A and 5B), members of superfamily of phase II detoxifying enzymes that protect cells by catalyzing the conjugation reactions of toxic compounds, e.g. CDDP with GSH, to form corresponding GS-Pt conjugate (Allocati et al., 2018). We also note the elevated transcript level of platinum efflux transporters, e.g. MATE1/SLC47A1, which may account for the diminished renal platinum in kidney from Bi(TPP)-CDDP co-administration group, yet the level of platinum influx transporters, e.g. OCT2/SLC22A2, was not significantly changed (Figure 5A). Therefore, GSTs and efflux transporters, e.g. MATE1/SLC47A1, may synergise to increase the discharge of GS-Pt conjugate from renal cell as suggested by both our data (Figures 2C and 5E) and previous reports (Tew and Gaté, 2001). In parallel, we demonstrate that Bi(TPP) lowers the CDDP-induced ROS in dose-dependent manner, which may be owing to the overexpression of alpha class GSTs, i.e., GSTA1, GSTA2, and GSTA3, that could provide antioxidant effect toward various ROS (Coles and Kadlubar, 2005; Simic et al., 2006).

Apoptosis is a mode of programmed cell death that is used by multicellular organisms to dispose of irreparably damaged cells and is executed by a family of caspases (Fuentes-Prior and Salvesen, 2004). CDDP-induced apoptosis occurs *via* activation of caspases, e.g. caspase 3, 8, and 9, in the apoptotic pathway (Cummings and Schnellmann, 2002; Henkels and Turchi, 1999). Our combined data reveal Bi(TPP) mediates the caspase cascade by either preventing the CDDP-induced caspases upregulation or directly inhibiting the caspase activity (Figures 6B, 6C, 6F, and S3E). The former may result from the hindered activation of apoptosis signaling pathways by less ROS (Redza-Dutordoir and Averill-Bates, 2016), which is mediated by Bi(TPP); the latter may be due to the binding of Bi(III) to cysteine residues at the caspase active site, because Bi(III) has been proven to inhibit enzyme activity through binding to the key cysteine in the active site (Wang et al., 2018).

Renal proximal tubules are largely dependent on ATP generation by mitochondrial oxidative phosphorylation and thus particularly susceptible to mitochondrial damage (Uchida and Endou, 1988; Wirthensohn and Guder, 1986). We find that Bi(TPP) promotes the generation of ATP, possibly due to Bi(TPP)-induced upregulation of cytochrome *c* (Figures 6B and 6C) and cytochrome *c* oxidase (encoded by COX8, complex IV) (Figure 5A and Table S2), both of which serve as indispensable parts of the mitochondrial electron transport chain (ETC). Cytochrome *c* is a multi-functional enzyme involved in life-sustaining functions, i.e., respiration and ROS scavenging, and in programmed cell death, i.e., apoptosis (Hüttemann et al., 2011). The increased cytochrome *c* may also account for the decreased of ROS level, because it was perceived as an "ideal antioxidant" (Pereverzev et al., 2003). Although, the dramatic increase of cytochrome *c* may slightly lead to cell apoptosis (Figure 6A), it may still contribute to scavenging generated ROS and preventing ATP depletion caused by CDDP (Figures 5C and 5D). We note that Bi(III) could bind to apo-form of

cytochrome *c* (Figures S6A and S6B); however, such binding did not trigger the activation of caspase cascade based on cell-free caspase activation assay (Figure S6C). It could be inferred that the binding of Bi(III) triggers certain feedback regulation to produce more cytochrome *c*. However, it is not clear why the significant upregulation of cytochrome *c* dose not initiate severe apoptotic cell death. This may be correlated with coherent upregulation of cytochrome *c* oxidase mediated by Bi(TPP) (Schüll et al., 2015), but the mechanistic insights of why cytochrome *c* is upregulated by Bi(TPP) and how it is regulated to be more "protective" here than apoptotic warrant further studies in the future.

A highly significant and clinically relevant finding of this study is that Bi(TPP) provides nephroprotection without compromising the antitumor effect of CDDP in an *in vivo* neuroblastoma orthotopic model. Bi(TPP) does not affect the therapeutic effectiveness of CDDP in either primary adrenal site or metastatic sites, e.g. lung and liver. Since some porphyrins e.g. 5, 10, 15, 20-tetra-(N-methyl-4-pyridyl)porphyrin [TMPyP4(P4)] and related manganese porphyrin (Han et al., 1999; Morris et al., 2012; Pradines and Pratviel, 2013) were reported to have anticancer activities when bound to G-quadruplex, it could be deduced that a nephroprotective metallo-porphyrin could exert certain degree of anticancer activity under rational design. N-acetylcysteine (NAC) has also been shown to display antitumor activity either used alone or combined with other anticancer drugs such as CDDP and doxorubicin (Delneste et al., 1997; Lopez et al., 2004; Muldoon et al., 2015). It is likely that $Bi(NAC)_3$ or its analogues could be further developed as a bifunctional partner of anticancer drugs upon optimization of pharmacokinetics and pharmacodynamics, so that they could simultaneously protect normal cells and synergize with an anticancer drug in its antineoplastic performance.

In summary, we demonstrate that Bi(TPP) could serve as a new type of potent protective agent against CDDP-induced nephrotoxicity without compromising its anticancer properties. Distinct from previously reported bismuth drugs that exert protective role through MT-dependent pathway, Bi(TPP) inactivates caspase-dependent apoptotic pathway, maintains energy supply, and eliminates the renal platinum. Our studies suggest that Bi(TPP) may be incorporated into CDDP-based chemotherapy regimens to ameliorate CDDP-induced nephrotoxicity in patients receiving low-dosed CDDP or those with refractory tumors receiving high-dosed CDDP. Our findings provide the potentials to revive the clinical usage of highly effective anticancer drug CDDP.

Limitations of the Study

Some limitations to the findings of this study must be acknowledged. First, we observed the demetallation of Bi(TPP) upon long period exposure to light and moisture. The enhancement of both stability and solubility of the complex in aquous medium either through structural or through compositional optimization would probably improve its *in vivo* protective potency. In addition, further optimization of pharmacokinetics profiles of the drug candidate may be required to achieve lower clearance and longer half-life while maintaining its promising potency and low toxicity. One additional limitation of the study is the difficulty in assessing precise protective mechanisms in primary human renal epithelial cells. Although we demonstrate that Bi(TPP) exerts an MT-independent protective action in HK-2 cell, more *in vitro* and *in vivo* assays are necessary to rule out cell-line-specific phenomenon. Further study is also required to unveil whether Bi(TPP) and/or other Bi(III) porphyrins as well as other protective metallo-porphyrins share the same or similar protective mode of action(s).

METHODS

All methods can be found in the accompanying Transparent Methods supplemental file.

DATA AND CODE AVAILABILITY

Data and code related to this paper may be requested from the authors. All the mRNA sequencing data could be found in Data S1.

SUPPLEMENTAL INFORMATION

Supplemental Information can be found online at https://doi.org/10.1016/j.isci.2020.101054.

ACKNOWLEDGMENTS

This work was supported by Innovation and Technology Fund, Hong Kong (ITS/124/17), Research Grants Council of Hong Kong SAR (R7070-18) and Norman & Cecilia Yip Foundation (University of Hong Kong).

We thank Kenneth Raymond (UC Berkeley) and Roman Vilar (Imperial College London) for helpful comments.

AUTHOR CONTRIBUTIONS

H.S., H.L., C-F.C., and Z.Z. conceived idea and designed experiments; R.W. synthesized the compounds; R.W. and S.Y. performed all the enzyme-based and cell-based experiments. R.M. and S.Y. conducted *in vivo* nephrotoxicity experiments. R.W. and Y.W. performed the transcriptomic analysis. C.C. performed the *in vivo* tumor model experiments. Y.Z. performed the pharmacokinetics study. R.W., H.L., and H.S. principally wrote the manuscript with input from all coauthors.

DECLARATION OF INTERESTS

H.S., C-F. C., R.W., C.C., and H.L. have filed a patent application (US Provisional Application No. 62/193,282) related to the Bi(III) compounds reported in this manuscript.

Received: October 28, 2019
Revised: March 10, 2020
Accepted: April 6, 2020
Published: May 22, 2020

REFERENCES

Allocati, N., Masulli, M., Di Ilio, C., and Federici, L. (2018). Glutathione transferases: substrates, inihibitors and pro-drugs in cancer and neurodegenerative diseases. Oncogenesis *7*, 8.

Arnott, J.A., and Planey, S.L. (2012). The influence of lipophilicity in drug discovery and design. Expert Opin. Drug Dis. *7*, 863–875.

Backman, J.T., Filppula, A.M., Niemi, M., and Neuvonen, P.J. (2016). Role of cytochrome P450 2C8 in drug metabolism and interactions. Pharmacol. Rev. *68*, 168–241.

Benet, L. (1991). Safety and pharmacokinetics: colloidal bismuth subcitrate. Scand. J. Gastroenterol. *26*, 29–35.

Bertolini, G., Roz, L., Perego, P., Tortoreto, M., Fontanella, E., Gatti, L., Pratesi, G., Fabbri, A., Andriani, F., and Tinelli, S. (2009). Highly tumorigenic lung cancer $CD133^{+}$ cells display stem-like features and are spared by cisplatin treatment. Proc. Natl. Acad. Sci. U S A *106*, 16281–16286.

Boogaard, P.J., Slikkerveer, A., Nagelkerke, J.F., and Mulder, G.J. (1991). The role of metallothionein in the reduction of cisplatin-induced nephrotoxicity by Bi^{3+}-pretreatment in the rat in vivo and in vitro: are antioxidant properties of metallothionein more relevant than platinum binding? Biochem. Pharmacol. *41*, 369–375.

Candelaria, M., Garcia-Arias, A., Cetina, L., and Dueñas-Gonzalez, A. (2006). Radiosensitizers in cervical cancer. Cisplatin and beyond. Radiat. Oncol. *1*, 15.

Chan, S., Wang, R., Man, K., Nicholls, J., Li, H., Sun, H., and Chan, G.C.-F. (2019). A novel synthetic compound, bismuth zinc citrate, could potentially reduce cisplatin-induced toxicity without compromising the anticancer effect through enhanced expression of antioxidant protein. Transl. Oncol. *12*, 788–799.

Cheng, L., Albers, P., Berney, D.M., Feldman, D.R., Daugaard, G., Gilligan, T., and Looijenga, L.H. (2018). Testicular cancer. Nat. Rev. Dis. Primers. *4*, 29.

Chevalier, R.L. (2016). The proximal tubule is the primary target of injury and progression of kidney disease: role of the glomerulotubular junction. Am. J. Physiol. Renal. *311*, F145–F161.

Coles, B.F., and Kadlubar, F.F. (2005). In Human Alpha Class Glutathione S-transferases: Genetic Polymorphism, Expression, and Susceptibility to Disease. Methods Enzymol, H. Sies and L. Packer, eds. (Academic Press), pp. 9–42.

Cummings, B.S., and Schnellmann, R.G. (2002). Cisplatin-induced renal cell apoptosis: caspase 3-dependent and-independent pathways. J. Pharmacol. Exp. Ther. *302*, 8–17.

Cun, S., Li, H., Ge, R., Lin, M.C., and Sun, H. (2008). A histidine-rich and cysteine-rich metal-binding domain at the c terminus of heat shock protein a from *Helicobacter Pylori* implication for nickel homeostasis and bismuth susceptibility. J. Biol. Chem. *283*, 15142–15151.

Cvitkovic, E. (1998). Cumulative toxicities from cisplatin therapy and current cytoprotective measures. Cancer Treat. Rev. *24*, 265–281.

De Luca, A., Parker, L.J., Ang, W.H., Rodolfo, C., Gabbarini, V., Hancock, N.C., Palone, F., Mazzetti, A.P., Menin, L., Morton, C.J., et al. (2019). A structure-based mechanism of cisplatin resistance mediated by glutathione transferase P1-1. Proc. Natl. Acad. Sci. U S A *116*, 13943.

Delneste, Y., Jeannin, P., Potier, L., Romero, P., and Bonnefoy, J.-Y. (1997). N-acetyl-L-cysteine exhibits antitumoral activity by increasing tumor necrosis factor α-dependent T-cell cytotoxicity. Blood *90*, 1124–1132.

dos Santos, N.A.G., Rodrigues, M.A.C., Martins, N.M., and Dos Santos, A.C. (2012). Cisplatin-induced nephrotoxicity and targets of nephroprotection: an update. Arch. Toxicol. *86*, 1233–1250.

Dresow, B., Nielsen, P., Fischer, R., Wendel, J., Gabbe, E.E., and Heinrich, H.C. (1991). Bioavailability of bismuth from ^{205}Bi-labelled pharmaceutical oral Bi-preparations in rats. Arch. Toxicol. *65*, 646–650.

Fuentes-Prior, P., and Salvesen, G.S. (2004). The protein structures that shape caspase activity, specificity, activation and inhibition. Biochem. J. *384*, 201–232.

Fujiwara, Y., and Satoh, M. (2013). Protective role of metallothionein in chemical and radiation carcinogenesis. Curr. Pharm. Biotechnol. *14*, 394–399.

Godbout, J.P., Pesavento, J., Hartman, M.E., Manson, S.R., and Freund, G.G. (2002). Methylglyoxal enhances cisplatin-induced cytotoxicity by activating protein kinase Cδ. J. Biol. Chem. *277*, 2554–2561.

Gonzalez, V.M., Fuertes, M.A., Alonso, C., and Perez, J.M. (2001). Is cisplatin-induced cell death always produced by apoptosis? Mol. Pharm. *59*, 657–663.

Haas, K.L., and Franz, K.J. (2009). Application of metal coordination chemistry to explore and manipulate cell biology. Chem. Rev. *109*, 4921–4960.

Han, F.X., Wheelhouse, R.T., and Hurley, L.H. (1999). Interactions of $TMPyP_4$ and $TMPyP_2$ with quadruplex DNA. Structural basis for the differential effects on telomerase inhibition. J. Am. Chem. Soc. *121*, 3561–3570.

Hausheer, F.H., Shanmugarajah, D., Leverett, B.D., Chen, X., Huang, Q., Kochat, H., Petluru, P.N., and Parker, A.R. (2010). Mechanistic study of BNP7787-mediated cisplatin nephroprotection: modulation of gamma-glutamyl transpeptidase. Cancer Chemother. Pharmacol. *65*, 941–951.

Hayes, J.D., Flanagan, J.U., and Jowsey, I.R. (2005). Glutathione transferases. Annu. Rev. Pharmacol. Toxicol. *45*, 51–88.

Henkels, K.M., and Turchi, J.J. (1999). Cisplatin-induced apoptosis proceeds by caspase-3-dependent and-independent pathways in cisplatin-resistant and-sensitive human ovarian cancer cell lines. Cancer Res. *59*, 3077–3083.

Hong, Y., Lai, Y.-T., Chan, G.C.-F., and Sun, H. (2015). Glutathione and multidrug resistance protein transporter mediate a self-propelled disposal of bismuth in human cells. Proc. Natl. Acad. Sci. U S A *112*, 3211–3216.

Hüttemann, M., Pecina, P., Rainbolt, M., Sanderson, T.H., Kagan, V.E., Samavati, L., Doan, J.W., and Lee, I. (2011). The multiple functions of cytochrome c and their regulation in life and death decisions of the mammalian cell: from respiration to apoptosis. Mitochondrion *11*, 369–381.

Ishikawa, T., and Ali-Osman, F. (1993). Glutathione-associated cis-diamminedichloroplatinum(II) metabolism and ATP-dependent efflux from leukemia cells. Molecular characterization of glutathione-platinum complex and its biological significance. J. Biol. Chem. *268*, 20116–20125.

Jafari, R., Almqvist, H., Axelsson, H., Ignatushchenko, M., Lundbäck, T., Nordlund, P., and Molina, D.M. (2014). The cellular thermal shift assay for evaluating drug target interactions in cells. Nat. Protoc. *9*, 2100.

Kaegi, J.H., and Schaeffer, A. (1988). Biochemistry of metallothionein. Biochemistry *27*, 8509–8515.

Katsuda, H., Yamashita, M., Katsura, H., Yu, J., Waki, Y., Nagata, N., Sai, Y., and Miyamoto, K.-i. (2010). Protecting cisplatin-induced nephrotoxicity with cimetidine does not affect antitumor activity. Biol. Pharm. Bull. *33*, 1867–1871.

Klaassen, C.D., Liu, J., and Diwan, B.A. (2009). Metallothionein protection of cadmium toxicity. Toxicol. Appl. Pharm. *238*, 215–220.

Kondo, Y., Himeno, S., Satoh, M., Naganuma, A., Nishimura, T., and Imura, N. (2004). Citrate enhances the protective effect of orally administered bismuth subnitrate against the nephrotoxicity of cis-diamminedichloroplatinum. Cancer Chemother. Pharmacol. *53*, 33–38.

Koyner, J.L., Ali, R.S., and Murray, P.T. (2008). Antioxidants. Nephron Exp. Nephrol. *109*, e109–e117.

Kruidering, M., Van De Water, B., De Heer, E., Mulder, G.J., and Nagelkerke, J.F. (1997). Cisplatin-induced nephrotoxicity in porcine proximal tubular cells: mitochondrial dysfunction by inhibition of complexes I to IV of the respiratory chain. J. Pharmacol. Exp. Ther. *280*, 638–649.

Ladenstein, R., Pötschger, U., Valteau-Couanet, D., Luksch, R., Castel, V., Ash, S., Laureys, G., Brock, P., Michon, J., Owens, C., et al. (2020). Investigation of the role of dinutuximab beta-based immunotherapy in the SIOPEN high-risk neuroblastoma 1 trial (HR-NBL1). Cancers *12*, 309.

Leonhardt, K., Gebhardt, R., Mössner, J., Lutsenko, S., and Huster, D. (2009). Functional interactions of Cu-ATPase ATP7B with cisplatin and the role of ATP7B in the resistance of cells to the drug. J. Biol. Chem. *284*, 7793–7802.

Leussink, B.T., Baelde, H.J., den Berg, T.M.B.-v., de Heer, E., van der Voet, G.B., Slikkerveer, A., Bruijn, J.A., and de Wolff, F.A. (2003). Renal epithelial gene expression profile and bismuth-induced resistance against cisplatin nephrotoxicity. Hum. Exp. Toxicol. *22*, 535–540.

Li, H., and Sun, H. (2012). Recent advances in bioinorganic chemistry of bismuth. Curr. Opin. Chem. Biol. *16*, 74–83.

Lopez, C.A., Kimchi, E.T., Mauceri, H.J., Park, J.O., Mehta, N., Murphy, K.T., Beckett, M.A., Hellman, S., Posner, M.C., and Kufe, D.W. (2004). Chemoinducible gene therapy: a strategy to enhance doxorubicin antitumor activity. Mol. Cancer Ther. *3*, 1167–1175.

Maret, W. (2008). Metallothionein redox biology in the cytoprotective and cytotoxic functions of zinc. Exp. Gerontol. *43*, 363–369.

Morris, M.J., Wingate, K.L., Silwal, J., Leeper, T.C., and Basu, S. (2012). The porphyrin TmPyP4 unfolds the extremely stable G-quadruplex in MT3-MMP mRNA and alleviates its repressive effect to enhance translation in eukaryotic cells. Nucleic Acids Res. *40*, 4137–4145.

Muldoon, L.L., Wu, Y.J., Pagel, M.A., and Neuwelt, E.A. (2015). N-acetylcysteine chemoprotection without decreased cisplatin antitumor efficacy in pediatric tumor models. J. Neuro Oncol. *121*, 433–440.

Murugan, R., and Kellum, J.A. (2011). Acute kidney injury: what's the prognosis? Nat. Rev. Nephrol. *7*, 209.

Naganuma, A., Satoh, M., and Imura, N. (1987). Prevention of lethal and renal toxicity of cis-diamminedichloroplatinum(II) by induction of metallothionein synthesis without compromising its antitumor activity in mice. Cancer Res. *47*, 983–987.

Nakamura, T., Yonezawa, A., Hashimoto, S., Katsura, T., and Inui, K.-i. (2010). Disruption of multidrug and toxin extrusion MATE1 potentiates cisplatin-induced nephrotoxicity. Biochem. Pharm. *80*, 1762–1767.

Pabla, N., and Dong, Z. (2008). Cisplatin nephrotoxicity: mechanisms and renoprotective strategies. Kidney Int. *73*, 994–1007.

Pereverzev, M., Vygodina, T., Konstantinov, A., and Skulachev, V. (2003). Cytochrome c, an ideal antioxidant. Biochem. Soc. Trans. *31*, 1312–1315.

Pradines, V., and Pratviel, G. (2013). Interaction of cationic manganese porphyrin with G-quadruplex nucleic acids probed by differential labeling of the two faces of the porphyrin. Angew. Chem. Int. Ed. *52*, 2185–2188.

Quintanilha, J.C.F., de Sousa, V.M., Visacri, M.B., Amaral, L.S., Santos, R.M.M., Zambrano, T., Salazar, L.A., and Moriel, P. (2017). Involvement of cytochrome P450 in cisplatin treatment: implications for toxicity. Cancer Chemother. Pharm. *80*, 223–233.

Rabik, C.A., and Dolan, M.E. (2007). Molecular mechanisms of resistance and toxicity associated with platinating agents. Cancer Treat. Rev. *33*, 9–23.

Rades, D., Fehlauer, F., Bajrovic, A., Mahlmann, B., Richter, E., and Alberti, W. (2004). Serious adverse effects of amifostine during radiotherapy in head and neck cancer patients. Radiother.Oncol. *70*, 261–264.

Redza-Dutordoir, M., and Averill-Bates, D.A. (2016). Activation of apoptosis signalling pathways by reactive oxygen species. Biochim. Biophys. Acta *1863*, 2977–2992.

Renes, J., de Vries, E.G., Nienhuis, E.F., Jansen, P.L., and Müller, M. (1999). ATP- and glutathione-dependent transport of chemotherapeutic drugs by the multidrug resistance protein MRP1. Br. J. Pharmacol. *126*, 681–688.

Samimi, G., Safaei, R., Katano, K., Holzer, A.K., Rochdi, M., Tomioka, M., Goodman, M., and Howell, S.B. (2004). Increased expression of the copper efflux transporter ATP7A mediates resistance to cisplatin, carboplatin, and oxaliplatin in ovarian cancer cells. Clin. Cancer Res. *10*, 4661–4669.

Satoh, M., Naganuma, A., and Imura, N. (1988). Metallothionein induction prevents toxic side effects of cisplatin and adriamycin used in combination. Cancer Chemother. Pharm. *21*, 176–178.

Schüll, S., Günther, S., Brodesser, S., Seeger, J., Tosetti, B., Wiegmann, K., Pongratz, C., Diaz, F., Witt, A., and Andree, M. (2015). Cytochrome c oxidase deficiency accelerates mitochondrial apoptosis by activating ceramide synthase 6. Cell Death Differ. *6*, e1691.

Seiwert, T.Y., Salama, J.K., and Vokes, E.E. (2007). The chemoradiation paradigm in head and neck cancer. Nat. Rev. Clin. Oncol. *4*, 156.

Silver, D.P., Richardson, A.L., Eklund, A.C., Wang, Z.C., Szallasi, Z., Li, Q., Juul, N., Leong, C.-O., Calogrias, D., and Buraimoh, A. (2010). Efficacy of neoadjuvant cisplatin in triple-negative breast cancer. J. Clin. Oncol. *28*, 1145.

Simic, T., Pljesa-Ercegovac, M., Savic-Radojevic, A., Hadziahmetovic, M., and Mimic-Oka, J. (2006). Identification of a glutathione S-transferase without affinity for glutathione sepharose in human kidney. Amino Acids *30*, 495–498.

Sprowl, J., van Doorn, L., Hu, S., van Gerven, L., de Bruijn, P., Li, L., Gibson, A., Mathijssen, R., and Sparreboom, A. (2013). Conjunctive therapy of cisplatin with the OCT2 inhibitor cimetidine: influence on antitumor efficacy and systemic clearance. Clin. Pharmacol. Ther. *94*, 585–592.

Tanihara, Y., Masuda, S., Katsura, T., and Inui, K. (2009). Protective effect of concomitant administration of imatinib on cisplatin-induced nephrotoxicity focusing on renal organic cation transporter OCT2. Biochem. Pharmacol. *78*, 1263–1271.

Tew, K.D., and Gaté, L. (2001). Glutathione S-transferases as emerging therapeutic targets. Expert Opin. Ther. Targets *5*, 477–489.

Thirumoorthy, N., Sunder, A.S., Kumar, K.M., Ganesh, G., and Chatterjee, M. (2011). A review of metallothionein isoforms and their role in pathophysiology. World J. Surg. Oncol. *9*, 54.

Uchida, S., and Endou, H. (1988). Substrate specificity to maintain cellular ATP along the mouse nephron. Am. J. Physiol. Renal. *255*, F977–F983.

Wang, D., and Lippard, S.J. (2005). Cellular processing of platinum anticancer drugs. Nat. Rev. Drug Discov. *4*, 307.

Wang, R., Lai, T.-P., Gao, P., Zhang, H., Ho, P.-L., Woo, P.C.-Y., Ma, G., Kao, R.Y.-T., Li, H., and Sun, H. (2018). Bismuth antimicrobial drugs serve as broad-spectrum metallo-β-lactamase inhibitors. Nat. Comm. *9*, 439.

Wirthensohn, G., and Guder, W.G. (1986). Renal substrate metabolism. Physiol. Rev. *66*, 469–497.

iScience, Volume *23*

Supplemental Information

Bismuth Porphyrin Antagonizes Cisplatin-Induced Nephrotoxicity *via* Unexpected Metallothionein-Independent Mechanisms

Runming Wang, Suyu Wang, Shing Chan, Yuchuan Wang, Yufeng Zhang, Zhong Zuo, Godfrey Chi-Fung Chan, Hongyan Li, and Hongzhe Sun

SUPPLEMENTAL FIGURES

Figure S1: Chemical structures of tested bismuth compounds for initial screening, Related to Figure 1

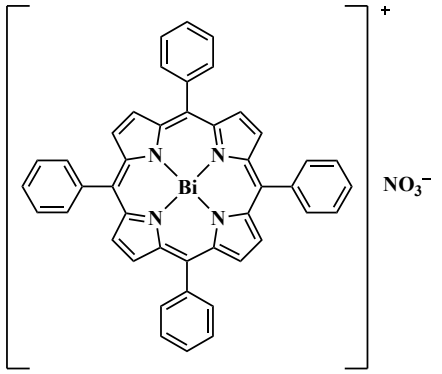

Cpd 1

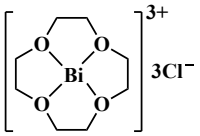

Cpd 2

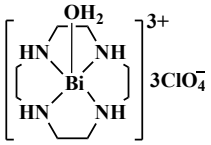

Cpd 3

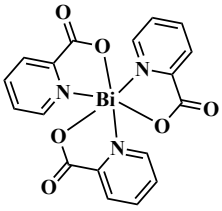

Cpd 4

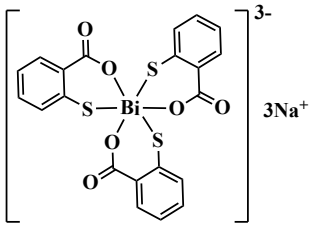

Cpd 5

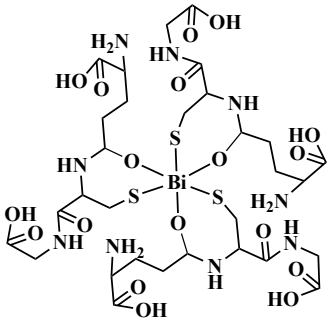

Cpd 6

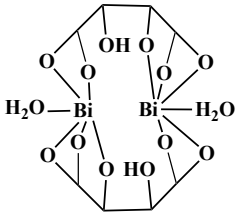

Cpd 7

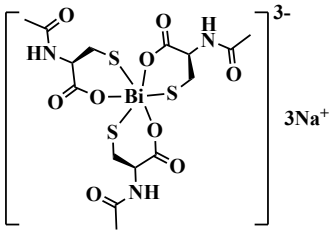

Cpd 8

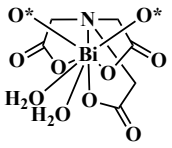

Cpd 9

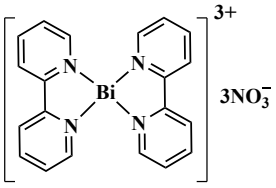

Cpd 10

* The two oxygens in Cpd 9 are from two adjacent molecules.

Figure S2: Cytotoxicity assay of Bi(III) compounds for initial screening, Related to Figure 1

(A-B) Dose-response curve showing the cytotoxicity of Bi(III) compounds by XTT assay upon treatment of (A) HK-2 and (B) MIHA cells at varying concentrations

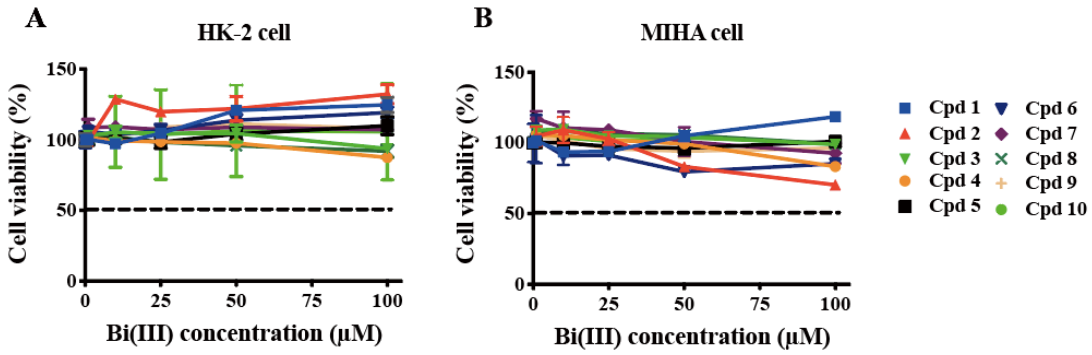

Figure S3: Transcriptome analysis of BiZn and detailed information on transcriptome analysis of Bi(TPP), Related to Figure 4

(A-B) Venn image and heat map of whole transcriptome sequencing on kidney extracts from mice receiving treatments of vehicle, BiZn, CDDP, or CDDP+ BiZn, respectively (n=3 mice per group). The overlapping sets amidst Venn image revealing that the expression of genes (A) in SET I was suppressed over CDDP-induced upregulation and (B) in SET II was induced over CDDP-induced downregulation upon the treatment of BiZn. Heat maps illustrate the scaled average gene expression. A false discovery cut-off rate of 0.05 was used for determining differential gene expression. Color code: Blue-low expression, red color-high expression. (C-D) Detailed child terms information from Fig. 4C, 4D. (C) showed endopeptidase activity+negative regulation of apoptotic signalling pathway and (D) showed inorganic cation transmembrane transporter activity+purine nucleotide metabolic process+calcium ion transport are shown in details. (E) The transcript level of genes enriched in TNF sigalling, p53 signalling, apoptosis and metabolic pathway according to the analysis in Figure 4E, 4F.

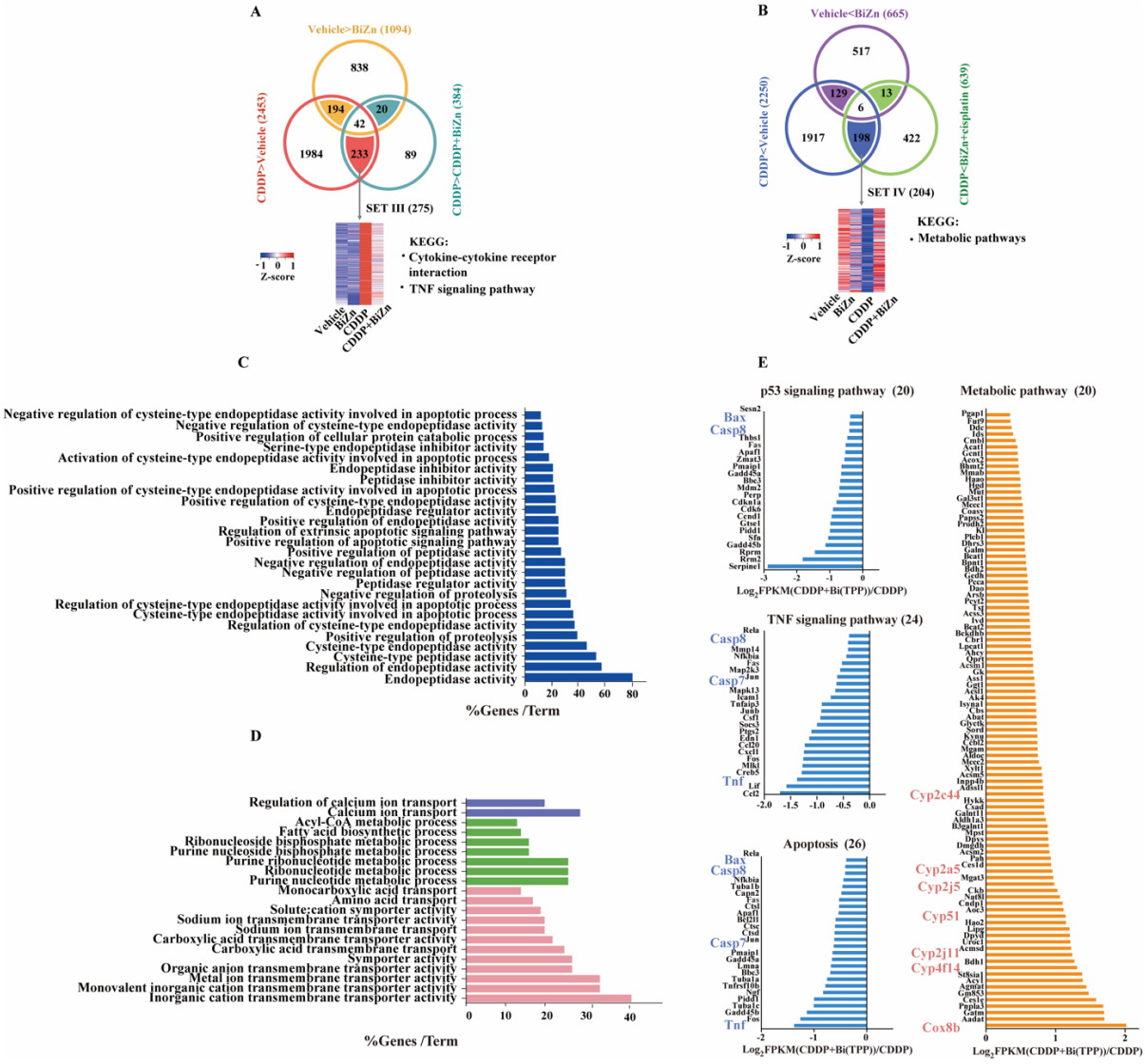
A
Vehicle>BiZn (1094)
838
194
20
42
1984
233
89
CDDP>Vehicle (2453)
CDDP>CDDP+BiZn (384)
SET III (275)
Z-score
KEGG:
• Cytokine-cytokine receptor interaction
• TNF signaling pathway
Vehicle
BiZn
CDDP
CDDP+BiZn
B
Vehicle<BiZn (665)
517
129
13
6
1917
198
422
CDDP<Vehicle (2250)
CDDP<BiZn+cisplatin (639)
SET IV (204)
Z-score
KEGG:
• Metabolic pathways
Vehicle
BiZn
CDDP
CDDP+BiZn
C
Negative regulation of cysteine-type endopeptidase activity involved in apoptotic process
Negative regulation of cysteine-type endopeptidase activity
Positive regulation of cellular protein catabolic process
Serine-type endopeptidase inhibitor activity
Activation of cysteine-type endopeptidase activity involved in apoptotic process
Endopeptidase inhibitor activity
Peptidase inhibitor activity
Positive regulation of cysteine-type endopeptidase activity involved in apoptotic process
Positive regulation of cysteine-type endopeptidase activity
Endopeptidase regulator activity
Positive regulation of endopeptidase activity
Regulation of extrinsic apoptotic signaling pathway
Positive regulation of apoptotic signaling pathway
Positive regulation of peptidase activity
Negative regulation of endopeptidase activity
Negative regulation of peptidase activity
Peptidase regulator activity
Negative regulation of proteolysis
Regulation of cysteine-type endopeptidase activity involved in apoptotic process
Cysteine-type endopeptidase activity involved in apoptotic process
Regulation of cysteine-type endopeptidase activity
Positive regulation of proteolysis
Cysteine-type endopeptidase activity
Cysteine-type peptidase activity
Regulation of endopeptidase activity
Endopeptidase activity
0 20 40 60 80
%Genes /Term
D
Regulation of calcium ion transport
Calcium ion transport
Acyl-CoA metabolic process
Fatty acid biosynthetic process
Ribonucleoside bisphosphate metabolic process
Purine nucleoside bisphosphate metabolic process
Purine ribonucleotide metabolic process
Ribonucleotide metabolic process
Purine nucleotide metabolic process
Monocarboxylic acid transport
Amino acid transport
Solute:cation symporter activity
Sodium ion transmembrane transporter activity
Sodium ion transmembrane transport
Carboxylic acid transmembrane transporter activity
Carboxylic acid transmembrane transport
Symporter activity
Organic anion transmembrane transporter activity
Metal ion transmembrane transporter activity
Monovalent inorganic cation transmembrane transporter activity
Inorganic cation transmembrane transporter activity
0 10 20 30 40
%Genes /Term
E
p53 signaling pathway (20)
Bax
Casp8
Log2FPKM(CDDP+Bi(TPP))/CDDP)
TNF signaling pathway (24)
Casp8
Casp7
Tnf
Apoptosis (26)
Bax
Casp8
Casp7
Tnf
Log2FPKM(CDDP+Bi(TPP))/CDDP)
Metabolic pathway (20)
Cyp2e44
Cyp2a5
Cyp2j5
Cyp51
Cyp2j11
Cyp4f14
Cox8b
Log2FPKM(CDDP+Bi(TPP))/CDDP)

Figure S4: Mitochondrial membrane potential (ΔΨm) of HK-2 cell affected by Bi(TPP) in the presence or absence of CDDP, Related to Figure 5

(A-B) Mitochondrial membrane potential of HK-2 cells exposed to various concentrations of Bi(TPP) (A) in the presence and (B) the absence of 20 µM CDDP. Data are represented as mean ± SEM. * p <0.05 ** p <0.01 and *** p <0.001, Student's t test, with the significance in comparison to the control group for (A) group of Bi(TPP) concentration at 0 µM for (B).

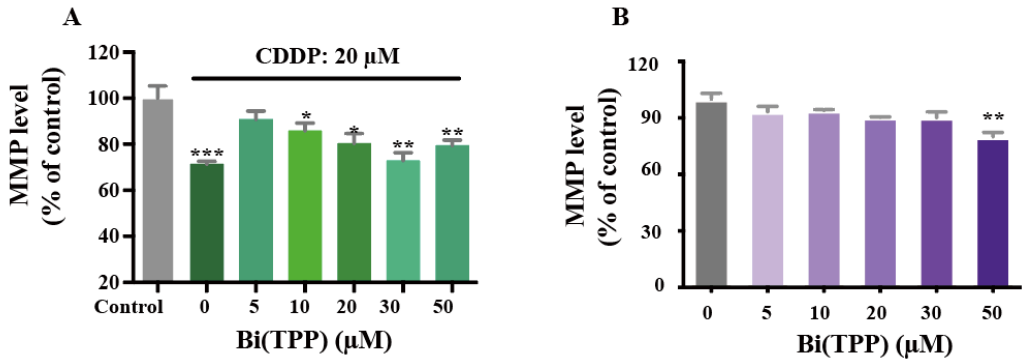

Figure S5: lysate activity of caspase 3 and caspase 9 inhibited by Bi(TPP), Related to Figure 6

(A-B) Examination of (A) caspase 3 and (B) caspase 9 activity from extracted lysate of HK-2 cells. M Data are represented as mean ± SEM. **p*<0.05 ***p*<0.01 and ****p*<0.001, Student's t test, with the significance in comparison to the group of Bi(TPP) concentration at 0 μM.

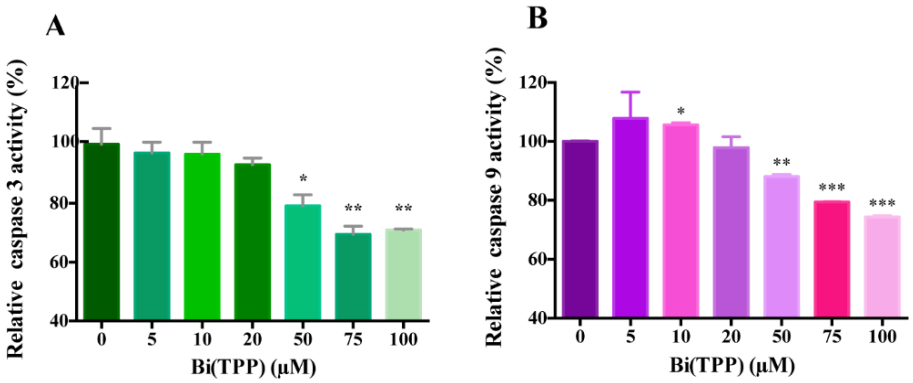

Figure S6: Characterization of the binding of Bi(III) ion to apo-cytochrome C, Related to Figure 6

(A) MALDI-TOF mass spectra of apo-form of cytochrome C (upper) and Bi-cytochrome C (lower) (B) Cellular thermal shift assays showing the binding of Bi(III) to (apo-)cytochrome C with ΔT_m = 13.54 ºC. (C) Representative immunoblots of fully-cleaved caspase 9 induced by apo-cytochrome c, Bi-cytochrome c and cytochrome c, respectively, from cell-free caspase activation assay.

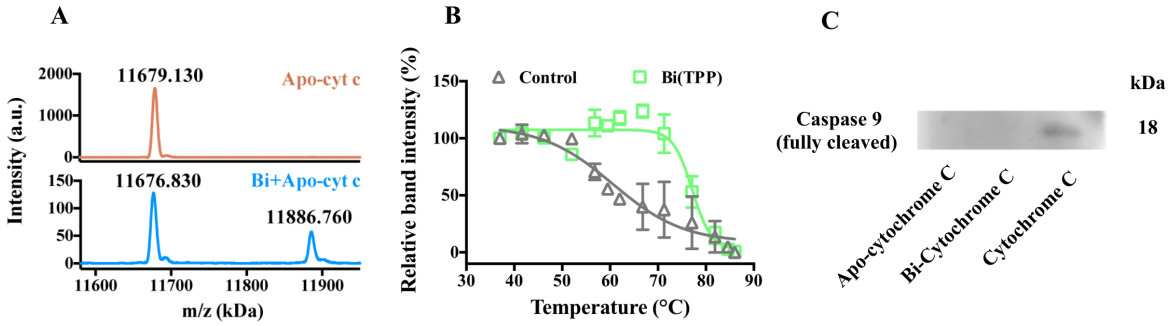

SUPPLEMENTAL TABLES

(Supplemental Tables 3 is provided elsewhere as Microsoft Excel files)

Table S1: Pharmacokinetics parameters of bismuth compounds in mouse plasma, Related to Figure 2

Compd.	BiZn* *p.o.* (96.46 mg kg^{-1})	Bi(TPP) *p.o.* (50 mg kg^{-1})
$AUC_{(0\text{-}8h)}$ (μg L^{-1} h)	78.3	104.2
$AUC_{(0\text{-}48h)}$ (μg L^{-1} h)	-	370.2
$T_{1/2}$ (h)	1.9	6.1
C_{max} (μg L^{-1})	24.7	16.8
T_{max} (h)	1.0	1.0
V_d/F (L)	151.9	113.4
CL/F (L^{-1} h)	10.9	6.6

*Data were generated from experiments in a previous report for comparison (Chan, Wang et al., 2019).

Table S2: Altered expression level of key gene upon drug treatment, Related to Figure 4

Gene name	Protein name	Fold change of averaged FPKM vs control				
		BiZn	Bi(TPP)	CDDP	BiZn +CDDP	Bi(TPP) +CDDP
Gsta1	Glutathione S-transferase, alpha 1	1.69	1.32	1.06	1.58	1.25
Gsta2	Glutathione S-transferase, alpha 2	1.55	1.47	0.83	1.04	0.92
Gsta3	Glutathione S-transferase, alpha 2	1.14	1.03	1.18	1.19	1.22
Gsta4	Glutathione S-transferase, alpha 4	1.12	0.87	0.64	1.76	0.88
Gstm5	Glutathione S- Transferase Mu 5	0.98	1.06	2.74	2.27	1.91
Gstm6	Glutathione S- Transferase Mu 6	1.25	1.42	2.33	3.22	2.46
Gstm7	Glutathione S- Transferase Mu 7	1.27	1.36	1.03	1.31	1.64
Mgst1	Microsomal glutathione S-transferase 1	1.08	0.95	2.13	2.76	1.78
Mgst2	Microsomal glutathione S-transferase 2	1.01	0.30	1.41	8.90	1.27
Mt1	Metallothionein 1	13.32	1.10	8.23	19.73	4.51
Mt2	Metallothionein 2	24.49	1.06	18.91	42.06	8.08
Oct 2/ Slc22a2	Solute carrier family 22 (organic cation transporter), member 2	0.95	0.61	0.99	0.65	0.76
Atp7a	ATPase, Cu^{2+} transporting, alpha polypeptide	0.93	1.08	0.85	1.33	0.98
Atp7b	ATPase, Cu^{2+} transporting, beta polypeptide	0.92	0.68	0.91	0.55	0.90
Mate1/ Slc47a1	Solute carrier family 47, member 1	1.01	0.55	1.12	0.64	0.80
Cyp2c44	Cytochrome P450, family 2, subfamily c, polypeptide 44	1.19	0.48	0.98	0.70	0.85
Cyp2a5	Cytochrome P450, family 2, subfamily a, polypeptide 5	1.96	0.29	3.25	0.35	0.57
Cyp2j5	Cytochrome P450, family 2, subfamily j, polypeptide 5	1.00	0.35	0.94	0.52	0.69
Cyp51	Cytochrome P450, family 51	0.85	0.13	0.84	0.18	0.30

Cyp4f14	Cytochrome P450, family 4, subfamily f, polypeptide 14	0.83	0.18	0.70	0.37	0.46
Cox8b	Cytochrome c oxidase subunit VIIIb	0.58	0.40	0.74	1.90	1.62

Table S4: GO term of biological process annotation for SET II, Related to Figure 4

GO ID	Go term	Term P Value	Group P Value	GO Groups	Associated Genes %	Genes
GO:0009062	Fatty acid catabolic process	7.492E-05	7.492E-05	Group00	10.91	12
GO:0030111	Regulation of Wnt signaling pathway	5.254E-04	5.254E-04	Group01	6.50	21
GO:0060349	Bone morphogenesis	4.826E-04	4.826E-04	Group02	8.96	12
GO:1901606	Alpha-amino acid catabolic process	1.601E-15	1.601E-15	Group03	24.47	23
GO:0008238	Exopeptidase activity	7.492E-05	7.492E-05	Group04	10.91	12
GO:0030900	Forebrain development	2.451E-04	2.451E-04	Group05	5.83	30
GO:0003279	Cardiac septum development	4.363E-05	4.363E-05	Group06	10.14	14
GO:0030182	Neuron differentiation	2.119E-04	2.119E-04	Group07	4.42	73
GO:0031175	Neuron projection development	3.194E-04	2.119E-04	Group07	4.69	56
GO:0048592	Eye morphogenesis	4.936E-04	4.936E-04	Group08	7.73	15
GO:0048593	Camera-type eye morphogenesis	5.533E-05	4.936E-04	Group08	9.93	14
GO:0051924	Regulation of calcium ion transport	6.589E-04	3.086E-04	Group09	6.58	20
GO:0006816	Calcium ion transport	3.086E-04	3.086E-04	Group09	5.85	29
GO:0072006	Nephron development	1.959E-04	1.931E-04	Group10	8.43	15
GO:0072073	Kidney epithelium development	6.712E-04	1.931E-04	Group10	7.82	14
GO:0072009	Nephron epithelium development	5.518E-04	1.931E-04	Group10	8.82	12
GO:0042327	Positive regulation of phosphorylation	1.468E-04	1.468E-04	Group11	4.81	57
GO:0001934	Positive regulation of protein phosphorylation	4.355E-04	1.468E-04	Group11	4.71	53
GO:0043410	Positive regulation of MAPK cascade	3.803E-04	1.468E-04	Group11	5.56	33
GO:0001568	Blood vessel development	3.750E-09	3.750E-09	Group12	6.82	55
GO:0001525	Angiogenesis	9.481E-07	3.750E-09	Group12	6.70	39

GO:0048514	Blood vessel morphogenesis	3.999E-09	3.750E-09	Group12	7.16	50
GO:0045765	Regulation of angiogenesis	1.755E-04	3.750E-09	Group12	6.80	23
GO:0045766	Positive regulation of angiogenesis	6.781E-04	3.750E-09	Group12	7.50	15
GO:0006163	Purine nucleotide metabolic process	8.119E-05	3.627E-06	Group13	6.63	26
GO:0006633	Fatty acid biosynthetic process	1.084E-04	3.627E-06	Group13	9.33	14
GO:0009259	Ribonucleotide metabolic process	7.608E-05	3.627E-06	Group13	6.67	26
GO:0034032	Purine nucleoside bisphosphate metabolic process	2.639E-07	3.627E-06	Group13	13.56	16
GO:0006637	Acyl-coa metabolic process	4.993E-06	3.627E-06	Group13	13.13	13
GO:0033875	Ribonucleoside bisphosphate metabolic process	2.639E-07	3.627E-06	Group13	13.56	16
GO:0009150	Purine ribonucleotide metabolic process	4.969E-05	3.627E-06	Group13	6.95	26
GO:0006865	Amino acid transport	1.414E-05	1.942E-10	Group14	9.60	17
GO:0008514	Organic anion transmembrane transporter activity	6.526E-10	1.942E-10	Group14	11.69	27
GO:1905039	Carboxylic acid transmembrane transport	1.918E-09	1.942E-10	Group14	11.90	25
GO:0015718	Monocarboxylic acid transport	6.004E-04	1.942E-10	Group14	7.91	14
GO:0022890	Inorganic cation transmembrane transporter activity	2.399E-04	1.942E-10	Group14	5.15	42
GO:0015077	Monovalent inorganic cation transmembrane transporter activity	3.052E-06	1.942E-10	Group14	6.88	34
GO:0015293	Symporter activity	2.221E-13	1.942E-10	Group14	16.36	27
GO:0035725	Sodium ion transmembrane transport	6.257E-06	1.942E-10	Group14	9.05	20
GO:0046873	Metal ion transmembrane transporter activity	3.252E-04	1.942E-10	Group14	5.48	34

GO:0046943	Carboxylic acid transmembrane transporter activity	1.692E-09	1.942E-10	Group14	13.50	22
GO:0015294	Solute:cation symporter activity	3.673E-10	1.942E-10	Group14	17.12	19
GO:0015081	Sodium ion transmembrane transporter activity	4.749E-06	1.942E-10	Group14	9.22	20

Table S5: Top 20 KEGG Pathway annotation chart of SET I, Related to Figure 4

Pathway	ID	Gene count	count%	P-Value
p53 signaling pathway	mmu04115	20	29.41%	1.702E-11
TNF signaling pathway	mmu04668	24	21.82%	1.988E-11
Apoptosis	mmu04210	26	18.84%	3.899E-11
Osteoclast differentiation	mmu04380	20	15.50%	1.917E-07
Leishmaniasis	mmu05140	14	21.54%	8.844E-07
HTLV-I infection	mmu05166	28	10.11%	1.036E-06
Influenza A	mmu05164	21	12.35%	2.388E-06
Toxoplasmosis	mmu05145	16	14.29%	1.262E-05
Herpes simplex infection	mmu05168	21	10.19%	3.402E-05
Proteoglycans in cancer	mmu05205	21	10.19%	3.402E-05
Cytokine-cytokine receptor interaction	mmu04060	24	9.09%	4.032E-05
Tuberculosis	mmu05152	19	10.80%	4.643E-05
Hepatitis B	mmu05161	17	11.72%	5.572E-05
MAPK signaling pathway	mmu04010	23	9.06%	6.470E-05
Salmonella infection	mmu05132	12	15.38%	1.194E-04
Rheumatoid arthritis	mmu05323	12	14.81%	1.606E-04
NF-kappa B signaling pathway	mmu04064	13	13.13%	2.155E-04
Legionellosis	mmu05134	10	17.24%	2.500E-04
Hematopoietic cell lineage	mmu04640	12	13.79%	2.789E-04
Chagas disease (American trypanosomiasis)	mmu05142	13	12.62%	2.979E-04

Table S6: Top 20 KEGG Pathway annotation chart of SET II, Related to Figure 4

Pathway	ID	Gene count	count%	P-Value
Metabolic pathways	mmu01100	96	7.57%	2.869E-17
Butanoate metabolism	mmu00650	10	37.04%	2.442E-06
Valine, leucine and isoleucine degradation	mmu00280	12	21.05%	1.284E-05
Tryptophan metabolism	mmu00380	9	19.57%	5.768E-04
Rap1 signaling pathway	mmu04015	18	8.33%	1.698E-03
Arginine and proline metabolism	mmu00330	8	16.33%	3.748E-03
Pantothenate and CoA biosynthesis	mmu00770	5	26.32%	9.006E-03
Propanoate metabolism	mmu00640	6	19.35%	9.006E-03
beta-Alanine metabolism	mmu00410	6	18.75%	9.006E-03
Cysteine and methionine metabolism	mmu00270	7	14.89%	9.006E-03
Sulfur metabolism	mmu00920	4	36.36%	9.006E-03
Synthesis and degradation of ketone bodies	mmu00072	4	36.36%	9.006E-03
Focal adhesion	mmu04510	15	7.43%	9.006E-03
ECM-receptor interaction	mmu04512	9	10.84%	9.752E-03
Phenylalanine metabolism	mmu00360	5	21.74%	1.017E-02
Protein digestion and absorption	mmu04974	9	10.00%	1.453E-02
Glycine, serine and threonine metabolism	mmu00260	6	15.00%	1.480E-02
Biosynthesis of unsaturated fatty acids	mmu01040	5	17.86%	1.842E-02
Biosynthesis of amino acids	mmu01230	8	10.26%	1.903E-02
Glyoxylate and dicarboxylate metabolism	mmu00630	5	17.24%	1.903E-02

Table S7: List of primer sequences of genes in RT-PCR (5'-3'), Related to Figure 5

	Forward Primers	**Reverse Primers**
Gsta1	CCT GAT CTG ATT CCT CCC ATT C	TCA AGC TCC TCG ACG TAG TA
Gsta2	AGT GCC ATT TAG GAA CCA GAG	TCC TCA TTC CCT GCT CTA TCT
Gsta3	CCT TCT TCC CTC CTT CTC TTT G	TAA ACC CTG CTC ACC CTT TG
Gsta4	CTA ACT CTG GGC TTC CAT TCT C	CTT CGG GTC TGT ACC AAC TTC
Gstm5	ACT CCT ATT CAC CGA CCT TCT	GCC TCT CAC TGC ACT CAT TT
Mgst1	TCA GTA TCA CCA GTG TGT CTT G	GCC GTT GAG TAG AGG AAT GTA G
Mgst2	CTC TTG GTT CCA GGC AGA TAT T	CTT GGG CAG AGT CCA CAT AAA
Mt1a	CGC CTT ATA GCC TCT CAA CTT C	CCA GAA ACC TAG CAT CCC TTA C
Mt1a	CCC TCT TTC TTT CTC TGG TCA C	GGG CTC CGA ATA ACC TAG AAT G
Slc22a2	CGT GTT GCT GGT AGG AAT TAG A	ATC CCA AAG TGC TGG GAT TAG
Slc47a1	GCT CGG TAG TTT GTG GGA TAT T	AGC ATG GCT GAT GGA TCT TAT T
Cyp2c44	GCC CTC ACT AGC ACT TCT TAT C	CCT AGC ACC TGC TTC AAT TCT A
Cyp2a5	GAG GAG ATT GAT CGG GTG ATT G	CAT GGA TTA CAG CCT CCG TAT AG
Cyp2j5	GGG TGA AAG GGT ATG GGA TAA A	CAG AAG GCT ATG AGG GTA AGA AG
Cyp51	GTG TGT TGA CTG GAT TGC TTT G	CCC ACC TAC TGC CTC CTA ATA
Cyp4f14	CTG AGC GTG TAA GAA CCC TAT T	CCC AGC CAC TAC ATC TCA TTT
Cox8b	CTG AGT GAA CCT CTG CCT TAC	CAG GGA GAA TGA CCT CAG AAA T
Gadph	GGA GTG AGT GGA AGA CAG AAT G	GAG GGA CAC AAG GTT ACC ATA TAC

Table S8: List of primary antibodies, Related to Figure 6

Target Protein	Host	Manufacturer	Catalog Number
Caspase 3	Rabbit	Proteintech	19677-1-AP
Caspase 7	Rabbit	Proteintech	27155-1-AP
Bax	Rabbit	Proteintech	50599-2-LG
Bcl-2	Rabbit	Proteintech	12789-1-AP
Caspase 8	Rabbit	Abcam	ab138485
Caspase 9	Rabbit	Abcam	ab2324
P53	Rabbit	Abcam	ab31333
TNF alpha	Rabbit	Abcam	ab9739
Cytochrome c	Mouse	Abcam	ab9739
Metallothionein	Mouse	Abcam	ab12228
β-Actin	Rabbit	Cell Signaling Technology	4970S

TRANSPARENT METHODS

General Chemistry

All reagents and solvents were purchased from commercial sources and used without further purification. Bismuth subsalicylate (BSS) and bismuth subgallate hydrate (BSG) were purchased from Alfa Aesar. Colloidal bismuth subcitrate were kindly given from Livzon Pharmaceutical Group Inc. All the porphyrins were purchased from Frontier Scientific, Inc. Fe(TPP), Zn(TPP), Cu(TPP), Co(TPP), Mn(TPP), and Ga(TPP) were purchased from Chemson Industrial (Shanghai) Co., Ltd. All other chemicals were purchased from Sigma-Aldrich unless otherwise stated. Chemical structure and CLog*P* were generated by ChemDraw Ultra 16.0. Specific primers for RT-PCR were purchased from Integrated DNA Technologies (IDT) and the sequences were listed in **Table S7**. Sources and details of all antibodies are listed in **Table S8**. Caspase-3 (ab52314) and caspase-9 (ab52203) protein were purchased from Abcam Ltd.

Human renal proximal tubule cells (HK-2), human hepatic cells (MIHA) and neuroblastoma cell (SKNLP) cell lines were cultivated in Dulbecco's modified Eagle's medium (DMEM) supplemented with 10% fetal bovine serum (FBS), supplemented with penicillin (100 μg mL^{-1}) and streptomycin (100 μg mL^{-1}). Cells were maintained in a 37 °C incubator under a humidified atmosphere of 5% CO_2.

Six-to-eight-week-old female and male BALB/c nude mice were purchased from Charles River Laboratories, Inc. Six-to-eight-week-old male C57BL/6 were supplied by the Laboratory Animal Services Centre at The Chinese University of Hong Kong. All the mice were randomly caged and given free access to water and food. All animal procedures were approved by the Committee on the Use of Live Animals in Teaching and Research (CULATR) of the University of Hong Kong (CULATR 4753-18) and the Animal Ethics Committee of the Chinese University of Hong Kong (Animal Experimentation Ethics Committee No.: 17/176/MIS-5-C). All animal procedures were approved by the Committee on the Use of Live Animals in

Teaching and Research (CULATR) of the University of Hong Kong (CULATR 4753-18) and the Animal Ethics Committee of the Chinese University of Hong Kong (Animal Experimentation Ethics Committee No.: 17/176/MIS-5-C).

Synthesis of Cpd 1 [Bi(TPP)] and Bi(THPP).

Bi(TPP) and Bi(THPP) were synthesized using a modified method (Wang, Lai et al., 2018). Briefly, $Bi(NO_3)_3 \cdot 5H_2O$ (1.99 g) was added to 80 mL of refluxing pyridine containing 0.10 g of the ligand (TPP: tetraphenylporphyrin or THPP: tetra(4-hydroxyphenyl)porphyrin), and a further 2.00 g of $Bi(NO_3)_3 \cdot 5H_2O$ was then added three hours later. Large amount of pyridine was removed by rotary evaporation after further refluxing for 2 hours and the resulting filtrate was then left to dry overnight under vacuum. Green solids that were obtained were then washed with chloroform and rotary evaporated to ensure all pyridine solvent was removed. The dark green solids were then purified on a silica gel column. The compound was purified by washing the column with firstly chloroform and then chloroform: methanol in a ratio of 20:1.

Bi(TPP): ^{1}H NMR (300 MHz, $CDCl_3$, δ ppm): 8.85 (s, 8H), 8.26 (dd, 8H, J= 7.43, 1.90 Hz), 7.79 (m, 8H), 7.23 (m, 4H). FAB-MS m/z +ve: 820.9 (calc: 821.2; $[BiL]^+$, 100%).

Bi(THPP): ^{1}H NMR (500 MHz, $CDCl_3$, δ ppm): 9.04 (s, 4H), 8.65 (s, 4H), 8.63 (s, 4H), 7.75 (t, 8H, J= 8 Hz). 6.99 (m, 8H). FAB-MS m/z +ve: 885.5 (calc: 885.2; $[BiL]^+$, 100%).

Synthesis of Cpd2.

The Bi(III) complex with 12-crown-4 was prepared using a modified method(Rogers, Bond et al., 1992). $BiCl_3$ (0.64 g, 2 mmol) was added to a mixture solvent of CH_3CN: CH_3OH=3: 1 (20 mL). The mixture was stirred for 2 hours at 60 ^oC, followed by the quick addition of 12-crown-4 (0.5 mmol in 80 μL). The mixture was continuously stirred for another 2 hours before centrifugation to remove a small quantity of white precipitates. The supernatant was slowly evaporated to remove about half of volume, followed by storage at 4 ˚C and -20 ˚C for 24 hours

and 48 hours, respectively. The resulting solution was further evaporated to afford crystalline material. The final product was collected before washed with large amount of ethanol.

^{1}H NMR (500 MHz, DMSO-d_6, δ ppm): 3.27 (s, 16H); ESI-MS m/z -ve: 457.2 (calc: 457.0; $[BiLCl_2]^-$, 100%).

Synthesis of Cpd3.

The Bi(III) complex with cyclen was prepared using a modified method (Luckay, Cukrowski et al., 1997). Bi_2O_3 (0.25 g) was stirred in 5 mL of 70% $HClO_4$ till totally dissolved, followed by the dropwise addition of cyclen (0.086 g, 0.5 mmol) in 5 mL 70% $HClO_4$. The mixture was continued to stir for 3 hours at 30 ^{o}C and then was slowly added appropriate amount sodium bicarbonate to adjust pH~1. The resulting solution was stood at 4 ^{o}C for 10 days and afforded small crystal by slow evaporation. The final product was collected before being washed by large amount of acetone and ethanol.

^{1}H NMR (500 MHz, DMSO-d_6, δ ppm): 3.11 (s, 16H), 7.95 (s, 4H); ESI-MS m/z -ve: 779.1 (calc: 779.0; $[Bi(ClO_4)_4]^-$, 100%)

Synthesis of Cpd 4.

The coordination of 2-picolinic acid to Bi(III) was carried out according to the literature (O. Anjaneyulu, 2010). $Bi(NO_3)_3 \cdot 5H_2O$ (0.49 g, 1.0 mmol) was added to deionized water (50 mL) resulting in a cloudy white solution. The temperature was increased until the solution was refluxing and had turned colorless. At this point, 2-picolinic acid (0.34 g, 3.0 mmol) was added and the resulting colorless solution was left to reflux for a further 2 hours. The solution was then allowed to cool to room temperature before being filtered under vacuum to remove any insoluble impurities. The colorless filtrate was then decanted into a beaker, covered and allowed to stand at room temperature for 2 days after which point a small amount of small, colorless crystals were collected.

^{1}H NMR (500 MHz, D_2O, δ ppm): 7.80 (s, 3H), 7.95 (d, 3H, J= 7.5 Hz), 8.10 (s, 3H), 8.82 (s, 3H); ESI-MS m/z +ve: 459.9 (calc: 461.0; $[(BiL_2)_2O]^{2+}$, 100%) ,452.9 (calc: 453.0; $[BiL_2]^+$, 6%)

Synthesis of Cpd 5.

To $Bi(NO_3)_3 \cdot 5H_2O$ (0.49 g) suspension in methanol (30 mL) was slowly titrated thiosalicylic acid (TSA) in methanol at room temperature till a transparent yellowish solution was formed. The solution was then filtered to remove any insoluble impurities and was then subjected to slow evaporation and the crystalline product was recrystallized from acetone-water.

^{1}H NMR (500 MHz, MeOD-d_4, δ ppm): 7.08 (t, 3H, 7.5 Hz), 7.26 (d, 3H, J= 8 Hz), 7.43 (td, 3H, J= 7.5, 1.5 Hz), 7.65 (s, 3H); ESI-MS m/z +ve: 515.3 (calc: 514.0; $[BiL_2+H]^+$, 100%), 666.9 (calc: 666.5; $[BiL_3+H]^+$, 34%).

Synthesis of Cpd 6.

To $Bi(NO_3)_3 \cdot 5H_2O$ (0.19 g) suspension in methanol (10 mL) was slowly added 30 mL methanol containing L-glutathione reduced (GSH, 0.26 g), sonicated and then stir at 60 ˚C for 4 hour. The solution was then filtered to remove any insoluble impurities and then slowly rotary evaporated to remove most solvents. Then the sample was freezed dry for overnight and the solid product was collected and washed by ethanol.

^{1}H NMR (500 MHz, DMSO-d_6, δ ppm): 2.02 (m, 6H), 2.36 (m, 6H), 3.70 (d, 6H, J= 5.5 Hz), 3.916 (s, 4H), 4.58 (dd, 4H, J= 14 Hz, 7.5 Hz), 8.31 (s, 12H); ESI-MS m/z -ve: 306.1 (calc: 306.0; L-H, 100%), 512.1 (calc: 512.3; $[BiL-3H]^-$, 29%), 818.9 (calc: 819.1; $[BiL_2-2H]^-$, 18%).

Synthesis of Cpd 7.

Bismuth tartrate was prepared based on according to the literature (Logutenko, Evseenko et al., 2003; Sagatys, Oreilly et al., 1992). $Bi(NO_3)_3 \cdot 5H_2O$ (0.48 g) was firstly dissolved in 5% HNO_3 under sonication, and then mixed with tartaric acid (0.45 g) for 2 hour at 60 ^oC. The pH of the

solution was adjusted to ~4 with $NaHCO_3$ till the white precipitate formed. The precipitate was filtered off, washed with large amount of distilled water and ethanol by centrifuge, and then dried in air. The product was then dissolved in minimum volume of diluted (3%) ammonia water and crystalline products were collected after several days' sedimentation.

^{1}H NMR (500 MHz, D_2O, δ ppm): 2.32 (d, 2H, J= 15.5), 2.45 (d, 2H, J= 15.5), 2.54 (s, 8H); ESI-MS m/z +ve: 711.0 (calc: 711.9; $[Bi_2L_2]^+$, 100%) , 748.9 (calc: 748.1; $[Bi_2L_2(H_2O)_2]^+$, 30%).

Synthesis of Cpd 8.

$Bi(NO_3)_3 \cdot 5H_2O$ (0.24 g, 0.5 mmol) and N-acetyl-L-cysteine (NAC, 0.24 g) were mixed in deionized water (10 mL) and left to stir at room temperature for 1 hour. To the resulting yellow solution was added NaOH (1 M, 3 mL) to raise the pH to ~ 6. The solution was then filtered to remove any insoluble impurities and was then subjected to freeze drier. The yellowish solid product was then washed with ethanol (6×10 mL) and dried in vacuum.

^{1}H NMR (500 MHz, DMSO-d_6, δ ppm): 1.76 (s, 9H), 4.26 (dt, 3H, J= 10.5 Hz, 5.5 Hz), 8.08 (d, 3H, J= 5 Hz); ESI-MS m/z +ve: 784.1 (calc: 784.5; $[BiL_3+4Na^+]^+$, 100%).

Synthesis of Cpd 9.

The preparation of Bi(III) complex with nitrilotriacetic acid (NTA) was carried out according to the literature (Summers, Abboud et al., 1994). To a boiling solution of NTA (0.21 g) in H_2O (50 mL) was added $(BiO)_2CO_3$ (0.42 g). The mixture was continued to stir for 18 hours. The solution was filtered while hot, and stored at 4 ^oC. The crystalline product was collected 1 day later and washed by saturated NaCl and ethanol.

^{1}H NMR (500 MHz, D_2O, δ ppm): 3.19 (s, 6H); ESI-MS m/z +ve: 398.0 (calc: 398.1; $[BiL+H]^+$, 100%).

Synthesis of Cpd 10.

The reaction of $Bi(N)_3.5H_2O$ with 2,2'-bipyridine was carried out according to the literature (Leonard J. Barbour, 1998). $Bi(NO_3)_3 \cdot 5H_2O$ (0.49 g, 1.0 mmol) and 2,2'-bipyridine (0.31 g, 2.0 mmol) were dissolved, with gentle heating, in a minimum amount of DMSO. Once fully dissolved, the warm colorless solution was filtered and the colorless filtrate was left to stand at room temperature for 14 days to allow a small amount of crystals. The crystalline product was then collected *via* vacuum filtration.

^{1}H NMR (500 MHz, DMSO-d_6, δ ppm): 7.36 (m, 2H), 7.63 (s, 2H), 7.69 (d, 2H, J = 1.5 Hz), 9.00 (s, 2H), 9.02 (m, 2H); ESI-MS m/z +ve: 488.9 (calc: 489.2; $[BiL(NO_3)_2]^+$, 100%).

Synthesis of Bi(TDHPP).

Tetra(3,5-dihydroxyphenyl) porphyrin (TDHPP) (0.074 g) was refluxed in DMF for 10 mins, followed by the addition of $Bi(NO_3)_3 \cdot 5H_2O$ (0.81 g) dissolved in minimal volume of ethylene glycol. The mixture was refluxed for 10 mins and filtered while hot. The filtrate was concentrated to *ca.* 3 mL, added to a 10 mL mixture of acetone/water (3: 10) and stored at 4 ˚C. Crystal-like product was washed and collected 4 days later.

^{1}H NMR (500 MHz, DMSO-d_6, δ ppm): 8.80 (s, 8 H), 8.74 (m, 8 H), 6.96 (dd, 8 H, J = 4 Hz, 6 Hz), 6.57 (m, 4H). ESI-MS m/z +ve: 949.4 (calc: 949.2; $[BiL]^+$, 100%)

Synthesis of Bi(TMPP) and Bi(TMOPP).

The Bi(III) complexes of tetra (4-methylphenyl) porphyrin (TMPP) and tetra (4-methoxyphenyl) porphyrin (TMOPP) were synthesized by a generic method. TMPP (0.064 g) was dissolved in pyridine (50 mL) and reflux for 1 hour. $Bi(NO_3)_3 \cdot 5H_2O$ (0.81 g) was added and the mixture continued to be refluxed for 5 hours, after which additional $Bi(NO_3)_3 \cdot 5H_2O$ (0.49 g) was added and the solution was refluxed overnight. Green products were collected and re-dissolved in chloroform after all the pyridine was removed in vacuum. The compound was purified by washing the column firstly with chloroform and then chloroform: methanol in the ratio of 8:1.

Bi(TMOPP) was prepared following the exactly same procedures by proportionally change the amount of raw material.

Bi(TMPP): ^{1}H NMR (300 MHz, $CDCl_3$, δ ppm): 9.13 (s, 8H), 8.61 (dd, 8H, J= 5.8 Hz, 1.7 Hz), 7.68 (tt, 4H, J= 7.7 Hz, 1.7 Hz), 7.29 (m, 10H), 2.72 (s, 12H). ESI-MS *m/z* +ve: 877.7 (calc: 877.3; $[BiL]^+$, 100%).

Bi(TMOPP): ^{1}H NMR (300 MHz, $CDCl_3$, δ ppm): 9.20 (s, 8H), 8.61 (m, 4H), 7.68 (tt, 2H, J = 7.7 Hz, 1.8 Hz), 7.33 (m, 2H) 7.29 (m, 10H), 4.12 (s, 12H). ESI-MS *m/z* +ve: 941.3 (calc: 941.8; $[BiL]^+$, 100%).

Synthesis of Bi(TPyP).

The preparation of complex 6 was based on a modified method[4]. $Bi(NO_3)_3 \cdot 5H_2O$ (0.20 g) was added to 30 mL pyridine and refluxed under vigorous stirring for 0.5 hours. Tetra (4-pyridyl) porphyrin (TPyP) (0.020 g) was added dropwise to the refluxed bismuth suspension and stirred for another 3 hours. Additional $Bi(NO_3)_3 \cdot 5H_2O$ (0.10 g) was added 3 and 6 hours later. The mixture was refluxed for another 16 hours, followed by evaporation to remove all pyridine. The resulting green solid was dissolved in the mixture of dichloromethane and methanol. Any impurity was filtered out and the product was then re-dissolved in ddH_2O. The solution was left at room temperature to allow the formation of crystals.

^{1}H NMR (500 MHz, $CDCl_3$, δ ppm): 9.02 (dd, 8H, J= 1.5 Hz, 4 Hz), 8.24 (s, 8H). 8.12 (dd, 8H, J= 1.5 Hz, 4.5 Hz). FAB-MS m/z +ve: 825.6 (calc: 825.5; $[BiL]^+$, 100%).

Synthesis of Bi(TClPP).

Tetra (4-chlorophenyl) porphyrin (TClPP, 0.075 g) was dissolved in pyridine (50 mL) and refluxed for 0.5 hours, followed by the addition of $Bi(NO_3)_3 \cdot 5H_2O$ (0.24 g). A further 0.24 g $Bi(NO_3)_3 \cdot 5H_2O$ was introduced 2 hours later and the mixture was refluxed for another 16 hours. Green gross product was collected and re-dissolved in dichloromethane after all the pyridine

was removed in vacuo. The compound was purified by washing the column with dichloromethane and then dichloromethane : methanol in a ratio of 20 : 1.

^{1}H NMR (500 MHz, DMSO-d_6, δ ppm): 8.80 (s, 8H), 8.25 (s, 4H), 8.17 (d, 6H, J= 1.5 Hz), 7.83 (d, 6H, J= 4.0 Hz). ESI-MS m/z +ve: 959.3 (calc: 959.1; $[BiL]^+$, 100%).

Synthesis of Bi(TDClPP).

Tetra (2,6-dichlorophenyl) porphyrin (TDClPP) (0.089 g) was dissolved in pyridine (50 mL) and refluxed for 2 hours, followed by the addition of $Bi(NO_3)_3 \cdot 5H_2O$ (0.48 g). A further 0.48 g $Bi(NO_3)_3 \cdot 5H_2O$ was introduced 4 hours later and the mixture was refluxed for another 48 hours. Green gross product was collected and re-dissolved in dichloromethane after all the pyridine was removed in vacuo. The compound was purified by washing the column firstly with dichloromethane and then dichloromethane: acetone in a ratio of 8:1. The product was collected by evaporation and washed with ethanol and saturated NaCl solution.

^{1}H NMR (500 MHz, DMSO-d_6, δ ppm): 8.69 (s, 8H), 7.98 (d, 8H, J = 1 Hz), 7.83 (dd, 4H, J = 7.5 Hz, 9.0 Hz). ESI-MS m/z +ve: 1096.9 (calc: 1096.9; $[BiL]^+$, 100%).

Synthesis of Bi(TAPP).

To 50 mL solvent mixture (pyridine: methanol: dichloromethane = 1:1:1), $Bi(NO_3)_3 \cdot 5H_2O$ (0.40 g) was added and refluxed under vigorous stirring for 0.5 hours. Tetra (4-aminophenyl) porphyrin (TAPP) (0.10 g) was slowly added to the refluxed suspension. Additional 0.4 g $Bi(NO_3)_3 \cdot 5H_2O$ was added 1 hour later and refluxed for another 3 hours. The mixture was refluxed for another 16 hours, followed by evaporation to remove all pyridine. Any impurity was filtered out and the resulting green solid was dissolved in the mixture of dichloromethane and methanol. Any impurity was filtered out and the product was then re-crystalized from methanol.

^{1}H NMR (500 MHz, DMSO-d_6, δ ppm): 8.81 (s, 8H), 7.79 (d, 8H, J= 15.5 Hz), 6.94 (d, 8Hh, J= 16.0 Hz), 5.49 (s, 8H). ESI-MS m/z +ve: 881.5 (calc: 881.3; $[BiL]^+$, 100%).

Synthesis of Bi(TSPP).

Tetra (4-sulfonatophenyl) porphyrin (TSPP) (0.124 g) was dissolved in 50 mL solvent mixture (pyridine: methanol = 3:1) and refluxed for 2 hours, followed by the addition of $Bi(NO_3)_3 \cdot 5H_2O$ (0.48 g). A further 0.48 g $Bi(NO_3)_3 \cdot 5H_2O$ was introduced 6 hours later and the mixture was refluxed for another 24 hours. Green gross product was collected and re-dissolved in acetone after all the pyridine was removed in vacuo. Final product was recrystallized from methanol.

^{1}H NMR (500 MHz, DMSO-d_6, δ ppm): 9.12 (m, 8H), 8.76 (m, 8H), 8.50 (m, 8H). ESI-MS m/z +ve: 1141.0 (calc: 1141.0; $[BiL+Na]^+$, 100%), 1163.0 (calc: 1163.1; $[BiL+2Na]^+$, 86%), 1185.1 (calc: 1185.0; $[BiL+3Na]^+$, 47%), 1228.9 (calc: 1228.9; $[BiL+4Na]^+$, 10%).

***In vitro* cell proliferation assay.**

The growth of HK-2 cells with supplementation of bismuth compounds and CDDP was measured using the cell proliferation kit II XTT assay (Roche Diagnostics, USA), according to the manufacturer's instruction. Ten to twenty thousand cells per well were grown in 96-well plates in a final volume of 100 μL culture medium per well overnight. For cytotoxicity assay, cells were then exposed to various concentrations (1-100 μM) of bismuth compounds for 24 hours. For primary screening of cytoprotective compounds, HK-2 and MIHA cells were treated with tested compounds at a fixed concentration (100 μM) for 2 hours and then exposed to CDDP treatment (10 μM) for 2 days. Various concentrations (1-100 μM) of Bi(TPP) and $Bi(NAC)_3$ were used for the dose-dependent assay under the same condition. Cells without drug treatment served as a control. After a fixed time of incubation, 50 μL of the XTT labeling mixture was added to each well, and the cells were further incubated for 4 hours under cell culture condition. The formation of formazan dyes, produced only by metabolic active cells, was spectrophotometrically detected at 490 nm. Measurements were performed in triplicate.

***In vivo* mouse model.**

Nephrotoxicity experiments were conducted with female BALB/c mice. A single nephrotoxic dose of CDDP (20 mg kg^{-1}) was *i.p.* injected into groups of mice on day 0. Bi(III) compounds (50 mg kg^{-1}) were *p.o.* pre-administered on day -2, -1 and 0 prior to CDDP administration and on day 2 and 4 post CDDP administration, respectively, as shown in **Fig. 2A**. Eight mice were used for each group and mice receiving vehicle (5% DMSO+10% PEG) served as control. The body weight of mice was monitored once daily and a scoring index of pathologic changes was given for each animal. Kaplan-Meier estimates of the survival curves were calculated and plotted. The examination of protective role of Bi(TMOPP) and Bi(TMPP) were performed under identical condition. For BUN assay, groups of mice were treated under the identical condition except that 6 mice were used in each group. All the mice were sacrificed on day 4 and serum of mice was collected and subjected to BUN assay (Urea Nitrogen Kit (serum), Stanbio Laboratory, USA) according to the manufacturer's instruction. Kidneys were dissected and acidified by 68% HNO_3 at 60 °C overnight using a Thermolyne DriBath. The samples were diluted to appropriate concentration for quantification of metals by ICP-MS (Agilent 7500a, Agilent Technologies, CA, USA) with ^{115}In as an internal standard. Metal quantifications were triplicated and average values were used.

Pharmacokinetic study was conducted with male C57BL/6 mice. A single dose of Bi(TPP) (50 mg kg^{-1}) was *p.o.* administered to groups of mice. Blood were collected by terminal cardiac puncture at 0.17, 0.33, 0.5, 1, 2, 8, 12, 48 hours post dose and kidneys were also collected at the time of sacrifice. Three mice were used for each time point. Blood samples were collected into heparinized tubes and centrifuged at 4000g for 5 min. Plasma and dissected tissues were acidified and subjected to ICP-MS measurement as mentioned above. Pharmacokinetic parameters, including the elimination half-life($t_{1/2}$), total clearance of drug from plasma (CL), volume of distribution (V_d), the area under the concentration-time curve to 8 hour (AUC_{0-8h}) and time curve to infinity ($AUC_{0-\infty}$), were calculated through noncompartmental analysis with

Phoenix WinNonlin (Certara). The area under the concentration-time curve to 8 hours was calculated through trapezoidal rule whereas $AUC_{(0-\infty)}$ was obtained from combining the area under the curve to the last time point $AUC_{(0-t)}$ with the extrapolated AUC value of the terminal phase. The value of C_{max} and T_{max} was evaluated through the individual dose-time profile.

Orthotopic neuroblastoma cancer xenograft model was established in male BALB/c nude mice using a modified method based on previously described methods[3]. Briefly, SKNLP neuroblastoma cells transfected with luminescent plasmid were injected into the adrenal glands of groups of mice and tumor was established within one month. Groups of tumor-bearing mice were p.o. pre-administered with vehicle and Bi(III) compounds (50 mg kg^{-1}), i.e., Bi(TPP), $Bi(NAC)_3$, BiZn, once per day on day –2, -1 and 0 prior to CDDP administration and every two days post CDDP administration, respectively. Mice received three times of CDDP administration (7.5 mg kg^{-1}) on day 0, 7 and 14 as shown in **Fig. 6A**. Four mice were used in vehicle, CDDP+vehicle, CDDP+$Bi(NAC)_3$, CDDP+Bi(TPP) group, one mouse in CDDP alone group died owing to the toxicity of CDDP during the experimental period; Five mice were used in CDDP+BiZn. Tumor-bearing mice receiving vehicle served as control. Mice were monitored twice daily and a scoring index of pathologic changes was given for each animal. Bioluminescence imaging was conducted on groups of mice once a week post CDDP administration. D-luciferin (150 mg kg^{-1}) was *i.p.* injected into each mouse. The growth of tumors was examined in real time by a luminescent IVIS imaging system, equipped with Living Imaging software (Xenogen, Alameda, CA). All the mice were sacrificed on Day 21, by an overdose of pentobarbital. Livers and lungs were dissected and subjected to bioimaging while the tumor size was collected for physical measurement.

Transcriptomics analysis.

Transcriptomics assay were performed according to previously described methods(Han, Zhang et al., 2018). Groups of mice were treated under the identical condition as described in

nephrotoxicity experiment except that all the mice were sacrificed 3 days post CDDP administration. Whole kidneys were collected and homogenized. Total RNA was isolated with RNeasy Mini Kit (Qiang, Venlo, USA). RNA purity was detected by NanoDrop® spectrophotometers (Thermo Fihser, MA, USA). RNA concentration was measured using Qubit® RNA Assay Kit in Qubit® 3.0 Flurometer (Life Technologies, CA, USA). RNA integrity was assessed using the RNA Nano 6000 Assay Kit of the Bioanalyzer 2100 system (Agilent Technologies, CA, USA).

For gene expression arrays, quality control and quantification of gene expression levels were performed with HTSeq v0.6.1(Anders, Pyl et al., 2015). Briefly, the initial preprocessing of the raw intensity data was firstly processed through in-house perl scripts to remove reads with low quality, and then FPKM of each gene was calculated based on the length of the gene and reads count mapped to this gene. FPKM stands for "fragments per kilobase of exon per million fragments mapped", and is calculated based on the length of the fragments and the reads count mapped to each fragment. Differential expression analysis between two groups (three biological replicates per condition) was performed using the DESeq R package (1.18.0)(Love, Huber et al., 2014). DESeq provides statistical routines for determining differential expression in digital gene expression data using a model based on the negative binomial distribution. The resulting *p*-values were adjusted using the Benjamini and Hochberg's approach for controlling the false discovery rate. Genes with an adjusted *p*-value < 0.05 found by DESeq were assigned as differentially expressed. Heatmaps were created using the Heatplus package in R and the average of the three replicates is shown.

Bioinformatic study.

GO terms and pathways in functionally organized networks were visualized with ClueGO(Bindea, Mlecnik et al., 2009). For the enrichment of biological terms and groups, we used the two-sided (Enrichment/Depletion) tests based on the hyper-geometric distribution.

Fusion criteria in ClueGO was selected to diminish the redundancy of the terms shared by similar associated proteins, which allows one to maintain the most representative parent or child term. The κ score threshold was set to 0.40. Other analysis parameters include: GO level intervals: (8-12); GO term minimum number of genes: 5; GO terms are presented as nodes and are clustered together based on the similarity of genes present in each term or pathway. Nodes with multiple colors are associated with more than one processes. R functions (phyper and *q*-value) were used to test for the statistical enrichment of the differentially expressed genes among the Kyoto Encyclopedia of Genes and Genomes (KEGG) pathways. KEGG pathways with corrected *p* value less than 0.05 were considered to be significantly enriched among the differentially expressed genes. Bubble chart was created using the ggplot2 package in R(Wickham, 2011) and the average of the three replicates is shown.

Real-Time PCR.

Real-time PCR to measure gene expression levels in HK-2 cells was carried out according to previous report (Xu, Wang et al., 2019). About 1×10^6 HK-2 cells were treated with 10 μM BiTPP, respectively, for 12 hours. Cell receiving no treatment served as control group. Three replicates were prepared for each group being combined for total RNA extraction. Total RNA was extracted using RNA Extraction Kit (Takara, Japan) according to manufacturer's instructions with slight modifications and collected in 200 μL RNase-free water and stored at -80 ^{o}C. A NanoDrop 1000 spectrophotometer was used to check RNA quality and to estimate RNA concentration. Reverse transcription was performed using PrimeScriptTM RT Master Mix (Perfect Real Time, Takara, Japan) and the resulting cDNA was used as template for PCR. Real-Time PCR was conducted using TB GreenTM Premix Ex TaqTM (Takara, Japan) and specific primers (sequences are listed in **Table S7**) on StepOnePlus Real-Time PCR system (Applied Biosystems, USA). cDNA for each sample and the non-template control were used in the detection of each target gene. The transcription level of target genes was quantified using ΔΔCt method (Livak and Schmittgen, 2001). GAPDH was used as an endogenous control and expression of target genes was calculated relative to GAPDH expression.

Immunoblotting analysis and cellular thermal shift assay.

HK-2 cells were pre-treated with 40 μM Bi(TPP) for 18 hours and then treated with 20 μM CDDP for another 24 hours. Total protein concentration was quantified by BCA Protein assay Kit (Pierce BCA Protein Assay Kit, Thermo Fisher Scientific Ltd.). Proteins were electrophoresed onto 15% SDS-PAGE gel and transferred to polyvinylidene fluoride membrane (PVDF) membranes (Hybond-P, GE Healthcare), which was then incubated with primary antibodies listed in **Table S6** and secondary antibody, rabbit anti-rabbit or anti-mouse antibodies. The protein blots were visualized with a chemiluminescence reagent (Thermo Fisher Scientific Ltd.) by MyECL Imager (Thermo Scientific). For dose-dependent study, all the procedures were the same except that cells were treated with different concentrations of Bi(TPP) at 0, 5, 10, 20, 30, 50 μM in the absence of CDDP.

Cellular thermal shift assay was performed according to previously described method(Molina, Jafari et al., 2013). HK-2 cells were cultivated in the absence or presence of 50 μM Bi(TPP) for 18 hours. The cell pellets were harvested and resuspended in PBS. About one million cells were aliquoted into PCR tubes in a volume of 80 μL. Heat treatment was performed at the designated temperature ranging from 37 °C to 64 °C for 3 min in a 96-well thermal cycler. Samples were lysed through three freeze-thaw cycles in liquid nitrogen. Lysate was centrifuged at 20,000 × *g* at 4 °C for 20 min, and the resulting supernatant was subjected to immunoblotting analysis by using caspase 3 and caspase 7 antibodies as described above.

Enzyme activity assay.

The caspase activity was examined with QuantiFluo^{TM} Caspase 3 Assay Kit (DCS3-100, BioAssay Systems, USA) and Caspase 9 Assay Kit (ab65607, Abcam Inc., UK) by a modified method from manufacturer's instructions. For lysate activity assay, 1×10^5 HK-2 cells were treated with 0, 5, 10, 20, 30, 50, 75, 100 μM Bi(TPP), respectively, for 24 hours and then lysed by RIPA buffer [25 mM Tris Cl (pH 7.4), 0.1% SDS, 150 mM NaCl, 1% Nonidet P-40, 2 mM

DTT], followed by incubation on ice for 15 minutes. Cytosolic extract was collected by centrifuge (1min, 10,000 × *g*). One hundred μg protein was diluted in 100 μL assay buffer (CAB) [50 mM PIPES, 10% glycerol 10 mM DTT] in 96-well assay plate (Corning® 3603). To each well, 2 μL of DEVD-AFC (AFC: 7-amino-4-trifluoromethyl coumarin) substrate (50 μM final concentration) and 5 μL of LEHD-AFC substrate (200 μM final concentration) was added for caspase 3 and caspase 9 activity assay, respectively, and the plate was incubated at 37°C for 1 hour in the dark. For protein activity assay, 1 unit of recombinant caspase 3 protein (ab52101, Abcam Inc., UK) or 1 unit of recombinant caspase 9 protein (ab52203, Abcam Inc., UK) was added to each reaction while other conditions were kept identical. Fluorescence was determined on a plate reader (Beckman Coulter, DTX 880) with excitation (λ_{ex}) /emission (λ_{em}) of 400/490 nm and 405/505 nm for caspase 3 assay, and caspase 9 assay respectively.

Cell-based bioassay.

For the measurement of GST level, experiments were performed using GST activity assay kit (ab65326, Abcam Inc., UK) according to the manufacturer's instructions. Briefly, about 5×10^5 HK-2 cells were treated with 0, 5, 10, 20, 30, 50 μM Bi(TPP), respectively. After 18 hours incubation, cells were washed with cold PBS and resuspend in 100 μL of GST assay buffer. Cytosolic extract was collected by centrifuge at 4°C (15min, 10,000×g) and resulting supernatant was added in a 50-μL aliquot in a 96-well assay plate (Corning® 3603), then was added 5 μL of GSH to each sample and control well. Fifty μL of GST reaction mix (GST Substrate (CDNB) Solution: GST Assay Buffer = 1:49) were added afterwards. The luminescence was measured on SpectraMax® iD3 multi-mode microplate reader (Molecular Devices, USA) in a kinetic mode. The experiment was carried out in triplicate.

For the measurement of cellular ATP level, experiments were performed using CellTiter-Glo® Luminescent cell viability assay kit (Promega corporation, USA) according to manufacturer's instruction. Briefly, about 5×10^4 HK-2 cells were seeded in each well of a 96-

well assay plate (SPL® 13485) and then incubated with 0, 1, 2, 5, 10, 20, 30, 50 μM Bi(TPP) for two hours and then with 40 μM CDDP for another 18 hours. To an aliquot of 100 μL culture was added 100 μL of CellTiter-Glo reagent. The mixture was incubated at room temperature for 20 min and then the luminescence was measured on Synergy™ HTX multi-mode microplate reader (BioTek Instruments, USA). The experiment was carried out in triplicate.

For the measurement of ROS level, about 2×10^4 HK-2 cells were incubated with 0, 5, 10, 20, 30, 50 μM of Bi(TPP) for 2 hours in 96-well assay plate, and then incubated with 20 μM CDDP. After another 6-hour incubation, cells were washed with PBS and replenished with medium containing 10 μM CM-H2DCFDA (Thermo Fisher Scientific Ltd.), followed by incubation for 45 min at 37 °C in the dark. The labelled cells were washed and replenished with fresh medium. Fluorescence was determined with excitation (λ_{ex})/emission (λ_{em}) 490/520 nm. The experiment was carried out in triplicate.

For mitochondrial membrane potential (MMP) assay, 1×10^5 HK-2 cells were incubated with 0, 5, 10, 20, 30, 50 μM of Bi(TPP) for 2 hours in 96-well assay plate, and then incubated with 20 μM CDDP for another 16 hours. Tetramethylrhodamine, ethyl ester (Invitrogen™) at 1000 nM were added to cell in medium and the cells were returned to incubator and cultured for an additional 30 minutes. Cells were then washed with PBS/0.2% BSA and fluorescence was measured in the same loading buffer with Ex/Em 549/575 nm. The experiment was carried out in triplicate.

For cellular platinum uptake measurement, about 5×10^5 HK-2 cells were cultured in a 6-well plate and pre-incubated with 0, 5, 10, 20, 30, 50 μM of Bi(TPP) for 6 hours. Afterwards, 20 μM of CDDP were added into each well for another 12 hours. The incubated cells were washed 3 times with PBS and harvested. About 1.5×10^5 cells were dissolved in 60 μL nitric acid (68%, v/v) overnight and subsequently diluted to appropriate concentration with nitric acid (1%, v/v). The platinum content was then measured by ICP-MS as described above.

Flow cytometry.

Flow cytometry assay was performed by using Alexa Fluor 488 Annexin V/Dead Cell Apoptosis Kit (Invitrogen™) according to manufacturer's instructions. About 1×10^6 HK-2 cells were seeded in each well in 6-well plates and pre-treated with 40 μM Bi(TPP) or Zn(TPP) for 24 hours, followed by another 24-hour incubation in the absence or presence of 20 μM CDDP. Cell treated with 1% DMSO served as control. All the cells were trypsinized and washed three times with cold PBS. For each group, about 5×10^5 cells per 100 μL were resuspended in 1×annexin-binding buffer, and then 5 μL Alexa Fluor® 488 annexin V (Component A) and 1 μL 100 μg mL^{-1} PI working solution were added. After 15 min incubation at room temperature, all the stained cells were evaluated by flow cytometry with measurement of fluorescence emission at 530 nm and 575 nm and excitation at 488 nm.

MALDI-TOF mass spectrometer analysis.

The apo-cytochrome c was prepared by a modified method based on previous report (Fisher, Taniuchi et al., 1973). Briefly, 50 mg cytochrome c from bovine heart (Sigma, C2037) was dissolved in 8 ml H_2O, 2 ml of glacial acetic acid and then 10 ml of 2.0 % silver acetate was added, and the mixture was kept at 42 ˚C for 6 hours in the dark. The protein was precipitated with 10 volumes of acid-acetone (1 mL H_2SO_4 (5 N)/100 mL acetone) and washed by acid-acetone for three times. The protein was dialysed in 0.1 M sodium phosphate buffer (pH 7.0) for overnight, and then suspended in 1 ml of 0.2 M ammonium acetate at pH 5.0 containing 6 M guanidine HCl and 1 M dithiothreitol (DTT). The suspension was left for 6 hours at room temperature in the dark and was centrifuged to collect supernatant. The proteins in supernatant was concentrated and dialysed in the same buffer. The protein was collected and used immediately. Bi-cytochrome c was prepared by co-incubation of apo-cytochrome c (20 μM) and Bi(TPP) (100 μM) at 4 ^oC overnight.

MALDI-TOF MS with a 355 nm solid state laser (Bruker Daltonics, Germany) was employed for performing the mass spectrometry experiments. One µl of the protein sample was mounted on a modified stainless-steel sample plate using electrically conductive tapes (9713 XYZ-Axis; 3M, St. Paul, MN) and then overlaid with 1 µL of matrix solution (saturated sinapic acid in 50: 50= acetonitrile (ACN): H_2O). The plate was then introduced into the mass spectrometer, operating in a positive-ion reflectron mode. The mass resolution of ion peaks was recorded in the range of m/z 10,000–20,000. MS data was processed using FlexAnalysis (version 1.2, Bruker Daltonics).

Cell-free caspase activation.

Cytoplasmic extracts of HK-2 cells were prepared using Mitochondria Isolation Kit for Cultured Cells (Thermo Scientific™) according to manufacturer's instructions. The protein extracts were diluted in 10 mM HEPES buffer (pH 7.0) containing 5 mM EGTA, 50 mM NaCl, 2 mM $MgCl_2$, 1 mM DTT, 1 mM ATP, 1 mM dithiothreitol with the final concentration of 1 mg mL^{-1}. Apo-cytochrome c, Bi-cytochrome c and cytochrome c were added to the extract solution with final concentration of 10 µM. The components were mixed well and incubated at 37 °C for 4 hours and then subjected to western blot analysis.

SUPPLEMENTAL REFERENCES

Anders, S., Pyl, P.T., and Huber, W. (2015). HTSeq-a Python framework to work with high-throughput sequencing data. *Bioinformatics* (Oxford, England). 31, 166-169.

Bindea, G., Mlecnik, B., Hackl, H., Charoentong, P., Tosolini, M., Kirilovsky, A., Fridman, W.-H., Pagès, F., Trajanoski, Z., and Galon, J. (2009). ClueGO: a Cytoscape plug-in to decipher functionally grouped gene ontology and pathway annotation networks. *Bioinformatics* (Oxford, England). 25, 1091-1093.

Chan, S., Wang, R., Man, K., Nicholls, J., Li, H., Sun, H., and Chan, G.C.-F. (2019). A novel synthetic compound, bismuth zinc citrate, could potentially reduce cisplatin-induced toxicity without compromising the anticancer effect through enhanced expression of antioxidant protein. *Transl. Oncol.* 12, 788-799.

Fisher, W.R., Taniuchi, H., and Anfinsen, C.B. (1973). On the role of heme in the formation of the structure of cytochrome c. *J. Biol. Chem.* 248, 3188-3195.

Han, B., Zhang, Z., Xie, Y., Hu, X., Wang, H., Xia, W., Wang, Y., Li, H., Wang, Y., and Sun, H. (2018). Multi-omics and temporal dynamics profiling reveal disruption of central metabolism in *Helicobacter pylori* on bismuth treatment. *Chem. Sci.* 9, 7488-7497.

Leonard J. Barbour, S.J.B., Peter C. Junk, Matthew K. Smith (1998). Bidentate nitrogen base adducts of bismuth(III) nitrate. *Aust. J. Chem.* 51, 337-342.

Livak, K.J., and Schmittgen, T.D. (2001). Analysis of relative gene expression data using real-time quantitative PCR and the 2−ΔΔCT method. *Methods.* 25, 402-408.

Logutenko, O.A., Evseenko, V.I., Yukhin, Y.M., and Afonina, L.I. (2003). Precipitation of bismuth(III) tartrates from nitrate solutions. Russ. *J. Appl. Chem.* 76, 1-6.

Love, M.I., Huber, W., and Anders, S. (2014). Moderated estimation of fold change and dispersion for RNA-seq data with DESeq2. *Genome Biol.* 15, 550.

Luckay, R., Cukrowski, I., Mashishi, J., H. Reibenspies, J., H. Bond, A., D. Rogers, R., and D. Hancock, R. (1997). Synthesis, stability and structure of the complex of bismuth(III) with the nitrogen-donor macrocycle 1,4,7,10-tetraazacyclododecane. The role of the lone pair on bismuth(III) and lead(II) in determining co-ordination geometry. *J. Chem. Soc., Dalton Trans.* 901-908.

Molina, D.M., Jafari, R., Ignatushchenko, M., Seki, T., Larsson, E.A., Dan, C., Sreekumar, L., Cao, Y., and Nordlund, P. (2013). Monitoring drug target engagement in cells and tissues using the cellular thermal shift assay. *Science* 341, 84.

O. Anjaneyulu, T.K.P., K. C. Kumara Swamy (2010). Coordinatively polymeric and monomeric bismuth(III) complexes with pyridine carboxylic acids. *Dalton Trans.* 39, 1935-1940.

Rogers, R.D., Bond, A.H., Aguinaga, S., and Reyes, A. (1992). Complexation chemistry of bismuth(III) halides with crown ethers and polyethylene glycols. Structural manifestations of a stereochemically active lone pair. *J. Am. Chem. Soc.* 114, 2967-2977.

Sagatys, D.S., Oreilly, E.J., Patel, S., Bott, R.C., Lynch, D.E., Smith, G., and Kennard, C.H.L. (1992). Group 15 Metal complexes with carboxylic acids. Preparation and crystal structure of polymeric ammonium aquabis[(+)-tartrato(2-)]bismuthate(III) hydrate. *Aust. J. Chem.* 45, 1027-1034.

Summers, S.P., Abboud, K.A., Farrah, S.R., and Palenik, G.J. (1994). Syntheses and structures of bismuth(III) complexes with nitrilotriacetic acid, ethylenediaminetetraacetic acid, and diethylenetriaminepentaacetic acid. *Inorg. Chem.* 33, 88-92.

Wang, R., Lai, T.-P., Gao, P., Zhang, H., Ho, P.-L., Woo, P.C.-Y., Ma, G., Kao, R.Y.-T., Li, H., and Sun, H. (2018). Bismuth antimicrobial drugs serve as broad-spectrum metallo-β-lactamase inhibitors. *Nat. Comm.* 9, 439.

Wang, X., Zhang, X., Lin, J., Chen, J., Xu, Q., and Guo, Z. (2003). DNA-binding property and antitumor activity of bismuth(III) complex with 1,4,7,10-tetrakis(2-pyridylmethyl)-1,4,7,10-tetraazacyclododecane. *Dalton Trans.* 2379-2380.

Wickham, H. (2011). ggplot2. *WIREs Computational Statistics.* 3**,** 180-185.

Xu, X., Wang, H., Li, H., Hu, X., Zhang, Y., Guan, X., Toy, P.H., and Sun, H. (2019). S-Dimethylarsino-glutathione (darinaparsin®) targets histone H3.3, leading to TRAIL-induced apoptosis in leukemia cells. *Chem. Comm.* 55, 13120-13123.